

Conjunctive grid cells in the entorhinal cortex respond to location and head direction

Peter Hebden

March 21, 2019

Contents

1	Introduction	2
2	Background	3
2.1	Introduction	3
2.2	Head Direction Cells	4
2.3	Grid Cells	5
2.3.1	Gridness	6
2.3.2	Grid fields	6
2.4	Conjunctive Grid Cells	7
3	Methods	10
3.1	Data collection and fundamental methods	10
3.2	Software	10
3.3	Cell classification	10
3.4	Grid properties	11
3.5	Centre of Mass	11
3.6	Place by direction sampling bias correction (PxD)	12
3.7	Place Fields	12
3.8	Head direction properties	14
3.8.1	Polarplots	14
3.8.2	The mean resultant vector	14
3.8.3	The Rayleigh test	15
4	Results	15
4.1	Summary of all cells	15
4.2	Gridness and directionality depend on cell type	17
4.3	CoM vector direction and the HD vector for some cells are correlated after PxD correction	18
4.4	Place fields and grid shifts	22
5	Discussion	25
6	Future Work	26

7 Appendix	32
7.1 Summary	32
7.2 Correlation	33
7.3 Spike rate, spatial autocorrelation, and polar plots	35

Abbreviations

- CoM: centre of mass
- EC: entorhinal cortex
- HD: head direction
- MEC: medial entorhinal cortex
- PxD: place by direction

Abstract

In contrast to a hippocampal place cell, a grid cell has multiple firing fields with regular spacing that tessellates the environment with a hexagonal pattern. Directional grid cells (“conjunctive grid cells”) respond selectively to head direction and location. The results in this report suggest: (1) A spike rate map’s centre of mass vector (CoM) directionality is correlated with preferred head direction (HD) when specific thresholds for gridness, CoM vector magnitude, and HD vector magnitude are applied. However, simply increasing the gridness threshold does not increase correlation. (2) Global grid shifts of all fields contribute more to the magnitude of the centre of mass vector of a spike rate map than local shifts based on a small number of fields with high spike rates.

1 Introduction

The hippocampus provides a spatial framework for experience [27]. It receives inputs via the medial entorhinal cortex (MEC) from regions that encode spatial variables, such as location and head direction, to update a representation of current position and heading [12, 13, 21, 29, 35]. While hippocampal place cell firing is different in different environments, grid cell firing is similar, i.e. the topography of grid firing is similar between different environments [12].

Early studies of grid cells used rats, but grid cells were soon found in mice [11], bats [48], monkeys [16], and humans [9, 15, 18]. They appear to be widely conserved across mammalian evolution [34] and, by implication, critical for survival.

The regular structure of the grid field implicates the grid cell as part of a universal, path-integration-based spatial metric. They are used to understand relative position in space [13], but not direction. Head direction (HD) cells are responsive to

direction [30, 31, 44, 45] and like grid cells, they retain their basic firing properties across environments [34].

Conjunctive cells combine the characteristics of grid cells and HD cells concurrently [35]. A subset of the putative grid cell data analysed for this report shows that directional grid cell firing rates depend on the directional tuning of the cell and the spatial tuning of the cell, especially after specific thresholds are imposed.

This report presents an analysis of data collected from freely moving rats in a one meter square environment. The aim is to explore and visualise the data, determine what usually causes a rate map’s centre of mass to shift, identify the parameters for the subset of cells that probably are conjunctive grid cells, and to quantify how the firing rate of these cells depends on location in the grid field and head direction.

2 Background

2.1 Introduction

Circa 1970 John O’Keefe recorded from single neurons in a freely moving rat confined to a small environment. He discovered “place cells” in the hippocampus ... the firing of these cells was strongly related to the animal’s location [26]. Unlike grid cells, place cells do not respond to similar places in different environments. Inputs map randomly to place cells, so the animal can recognise the same place in the same environment, and not falsely recognise a similar place in a different environment, an ability known as pattern separation [49].

In 1978 O’Keefe and Nadel published the influential book “The hippocampus as a cognitive map” [27] where they argued that place cells are the physiological basis for the cognitive map hypothesized by Edward C. Tolman in the 1940s. However, place cells alone are not sufficient for navigation. The animal needs to have a sense of its relative location and direction, it needs other specialised cells.

Head direction cells were discovered in the dorsal presubiculum by James Ranck in 1984 [30, 31, 41, 42]. They are found throughout most layers of the MEC, but they are particularly abundant in the presubiculum [36].

Other cell types were also found in the entorhinal cortex. Grid cells were discovered by the Moser lab in 2004–2005 [12, 13], followed by the discovery of boundary vector cells [2], border cells in 2008 [38], and the progressive increase in grid scale

from dorsal to ventral MEC in the same year [5]. Speed cells were discovered in 2015 [17].

2.2 Head Direction Cells

Head-direction (HD) cells are a class of spatial cells found in the dorsal presubiculum and regions connected with the presubiculum, such as the anterior thalamus [30, 40, 41, 43]. In rats, they are abundant in the entorhinal cortex, mostly in layers III and V, and almost non-existent in layer II [35], as shown in Figure 1.

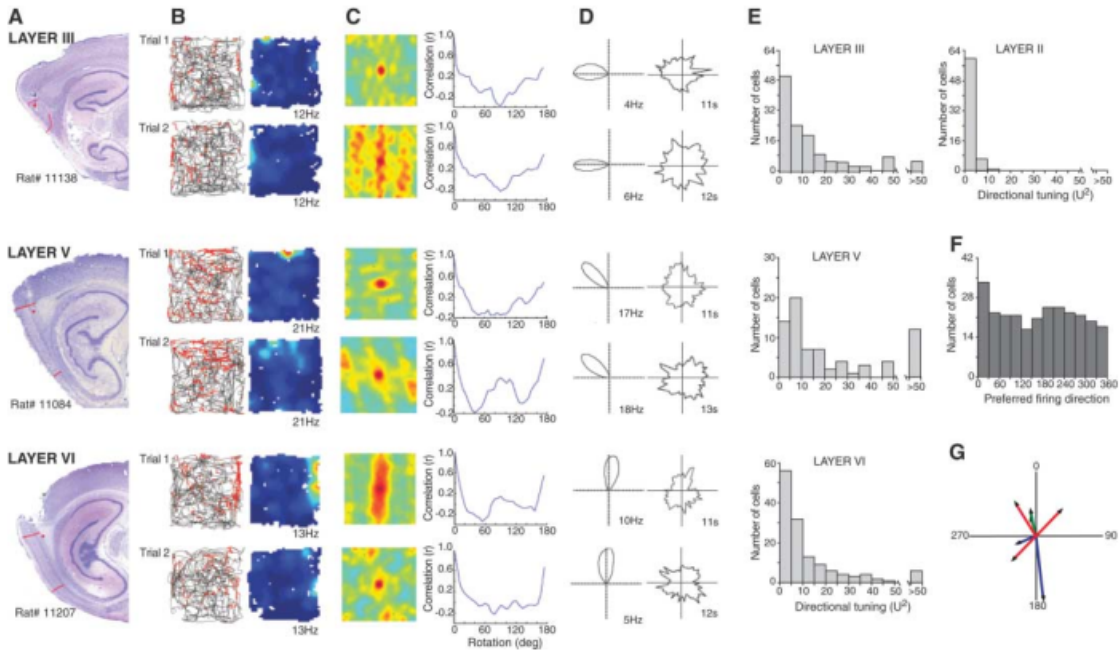


Figure 1: Head-direction cells are in layers III, V and VI of the entorhinal cortex. Image:[35].

They are tuned to fire when the rat's head points in a specific direction relative its environment, and as the rat moves the direction vectors are parallel, i.e. they do not converge on a fixed point. They care about the head's azimuthal orientation in the horizontal plane, but not about pitch and roll, body orientation, or movement. Unlike hippocampal place cells, the preferred direction is independent of location [6, 41].

The firing rate decreases sharply as head direction rotates away from the preferred direction, which ranges from about 60° to 140° wide, and $\sim 90^\circ$ on average. The distribution of peak firing directions across the population of cells is uniform.

2.3 Grid Cells

Grid cells are a type of pyramidal neuron that responds to relative location independent of external sensory cues and the specific environment; they are found in the entorhinal cortex [12] and exist in all principal layers of the MEC, an area of neocortex adjacent to the hippocampus, as shown in Figure 2.

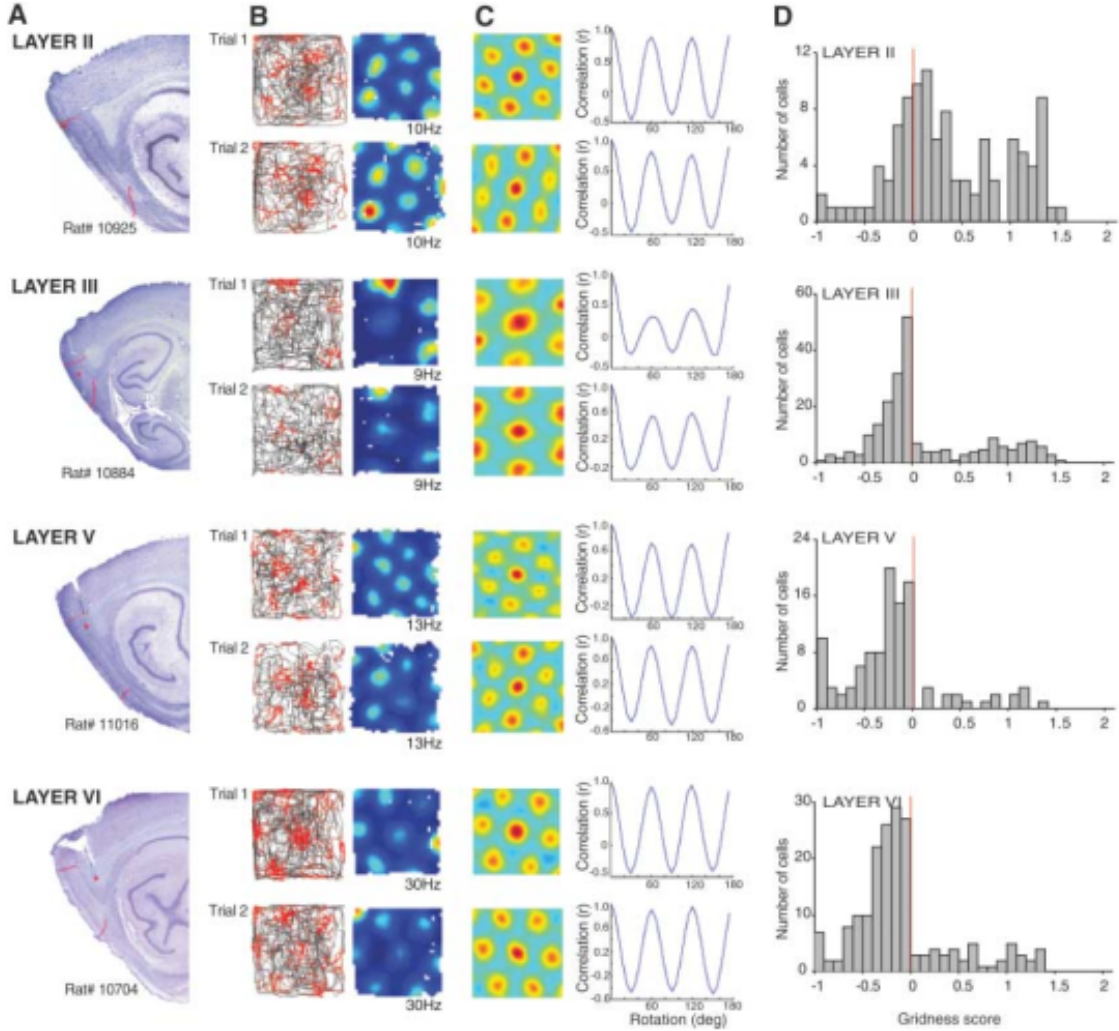


Figure 2: Grid cells exist in all principal cell layers of the medial entorhinal cortex. Image:[35].

When these cells were recorded in larger environments, a pattern emerged: their firing fields formed tessellating hexagonal grids of equilateral triangles [13]. Grid cells are defined by such periodic firing fields; this property can be quantified by a metric known as “gridness”.

2.3.1 Gridness

Gridness is a measure of spatial periodicity. The spatial autocorrelation pattern of a grid cell tends to have a 60° rotational symmetry, and the grid pattern will tend to be anti-correlated with itself when rotated by 30° , Figure 6(b). To obtain the gridness score, the spatial autocorrelation of the grid pattern was correlated with its rotated versions at 60° and 120° , while subtracting the correlation with the rotated versions at 30° , 90° , and 150° . This score was also used with small variations in [4, 19, 35, 38, 46]. Threshold values for grid cells are typically in the 0.3 to 0.4 range (on a scale from -1 to 1) [35].

2.3.2 Grid fields

Grid fields differ in terms of spacing, phase, and orientation [13].

- Grid spacing is the typical minimum distance between the centres of two consecutive grid fields. Grid cells in the dorsal MEC encode smaller spaces, while grid cells in the ventral MEC encode larger spaces [5].
- Grid phase is the offset of grid vertices relative to the x and y axes [13]; it can be defined by the position of a single firing rate peak [10].
- Grid orientation is the orientation (angle) of the grid axes relative to the local boundaries of the environment. Grid cells of similar spacing tended to have almost identical grid orientations within the same environment [39].

The properties of cells with grid fields varies with each MEC layer. Layer II contains the largest density of pure grid cells – their firing rate is not modulated by direction. Grid cells from deeper layers are intermingled with conjunctive cells [35] and head direction cells. Layers III, V and VI have cells with a grid-like pattern that fire only when the animal is facing a particular direction [35].

Cells in the MEC encode information about position and movement [35]. As an animal moves through space it uses *path integration* to keep track previous locations and maintain its sense of position independent of current visual inputs. Path integration probably depends on grid cells in the MEC [13].

2.4 Conjunctive Grid Cells

Some grid cells, “conjunctive grid cells”, also have HD properties. The proportion of such cells in the EC depends on the layer, as shown in Figure 3. Most grid cells in layer II are HD invariant, while those in the deeper layers usually have HD selectivity, some of which are pure HD cells. The proportion of directionally modulated cells in the deeper layers is $\sim 70\%$ [35].

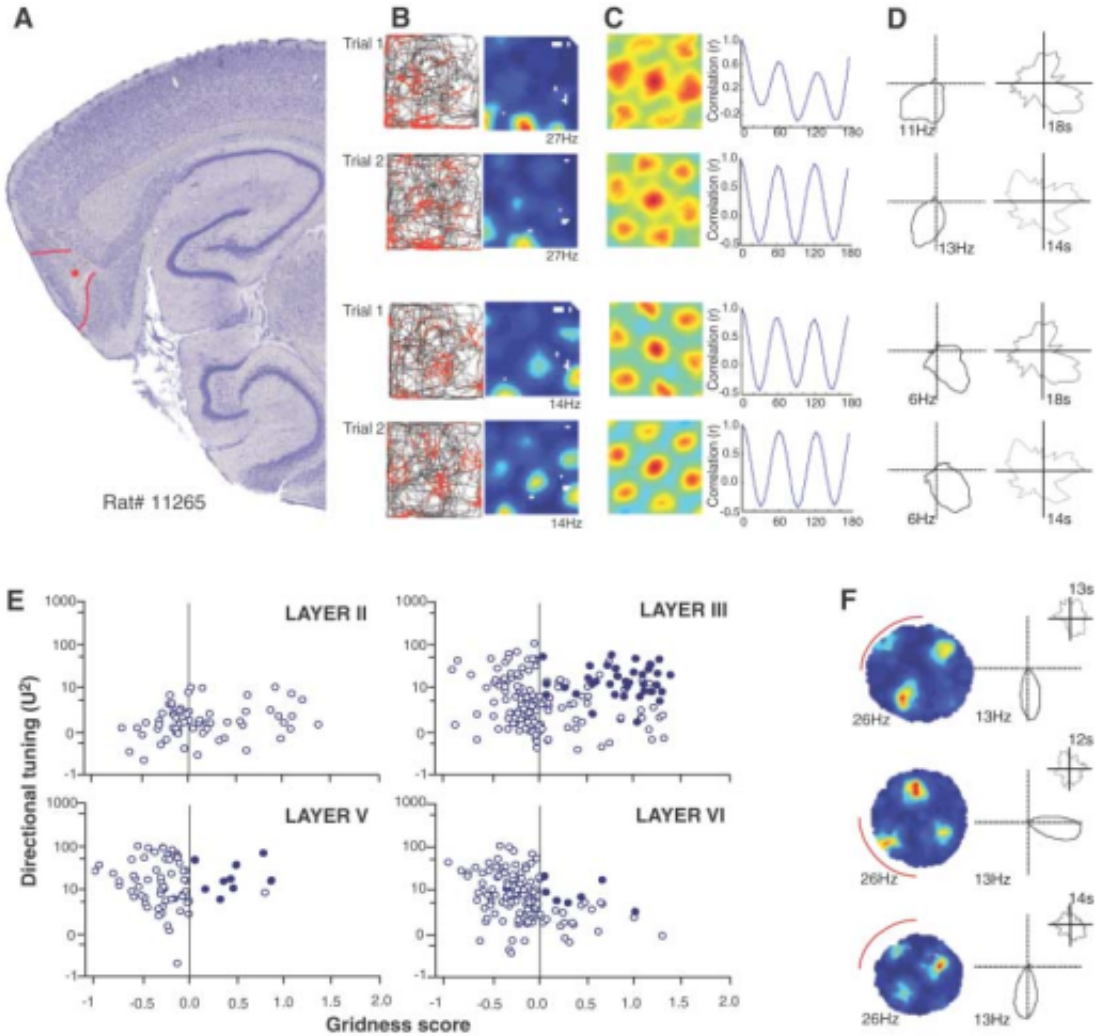


Figure 3: Conjunctive representation of position and direction. Image:[35].

An important property of HD cells is known as *obligatory coupling* – the angular distance between the preferred directions of pairs of HD cells is very resistant to change. So, after a cue is removed, if the preferred head direction of cell 1 rotates by $\sim 40^\circ$, cell 2 rotates by a similar amount [41, 42].

In Sargolini *et al.* (2006) they found that during environmental manipulations cells with different degrees of gridness and directionality always responded as a

coherent ensemble [35], e.g. during the rotation of a polarizing cue card as shown in Figure 4.

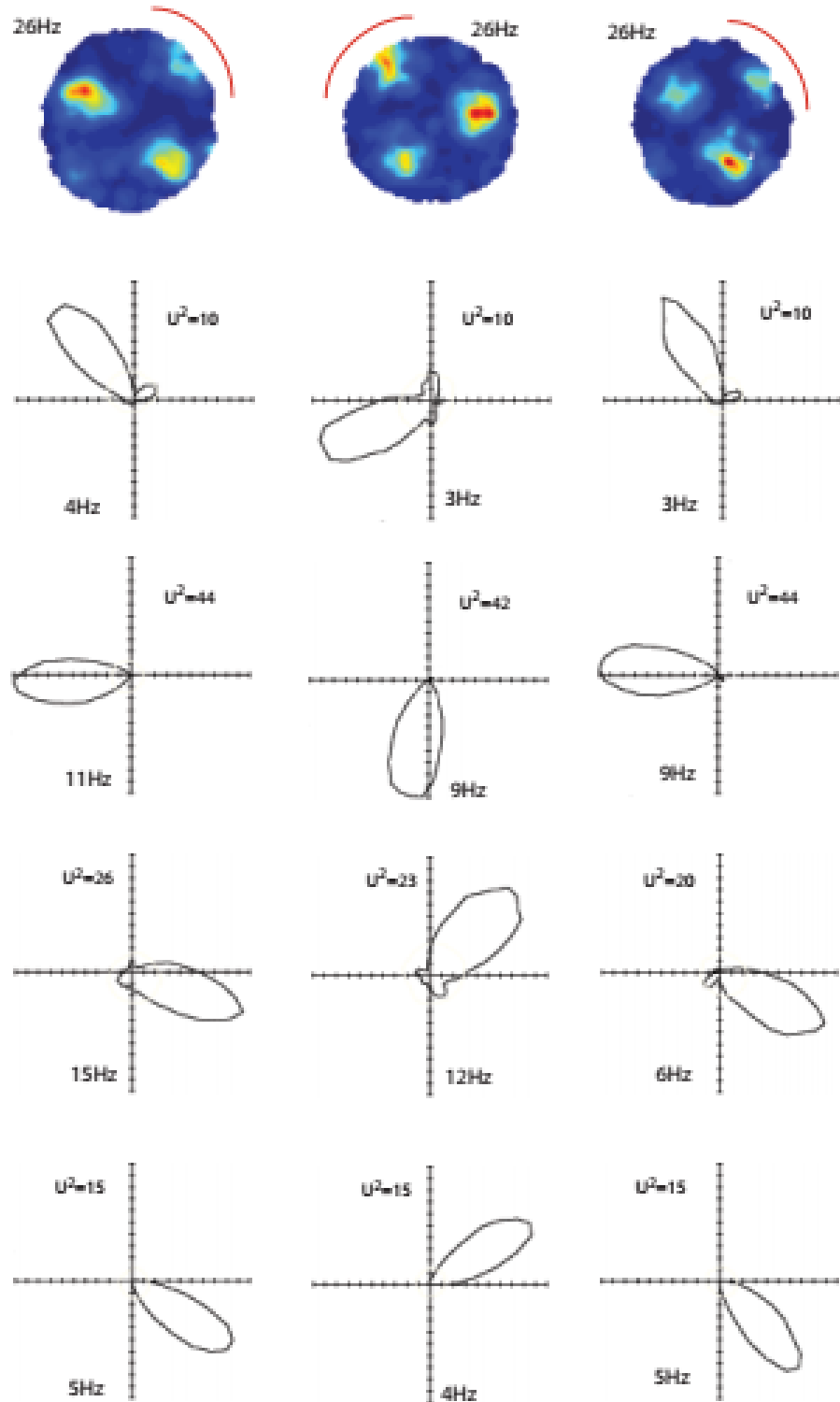


Figure 4: Grid cells and HD cells are coupled. Top row: Rate maps for one grid cell. Rows 2 to 4: polar plots for four representative head-direction cells. Recordings were made simultaneously in layer VI of MEC after rotation of a polarizing cue card on the wall of a circular environment. Columns one and three: cue card (red arc) is in the original position. Column two: cue card is rotated 90°. Image: [35].

The interaction of grid cells with other cell types in the MEC is not clear [35]. The interactions are probably complex because the the MEC is the hub of a widespread brain network for spatial navigation [12, 13, 14, 27, 28, 29, 32, 33, 37].

MEC layer II is dominated by grid cells and contains a two dimensional, ensemble-encoded metric map of relative spatial location [12, 13, 14] that is independent of the specific environment and the external sensory cues [35]. Grid cells co-localized with HD cells are in the deeper layers. Conjunctive grid cells are in the deeper layers of the MEC [35], and in the pre- and parasubiculum [4].

The preferred firing directions of directionally modulated grid cells in rat EC are aligned with the grids [9]. Figure 5, left panel, shows the firing rate heat map of a typical ‘conjunctive’ directional grid cell where firing rate is a function of the rat’s location within a 1 square meter box (red, high firing rate; blue, low rate; white, unvisited location; peak rate 3.1 Hz). The middle panel shows the spatial autocorrelogram for this heat map. The right panel shows this cell’s polar firing rate map. The black arrow indicates mean firing direction. Red lines indicate the main axes of the grid firing pattern identified from the spatial autocorrelogram.

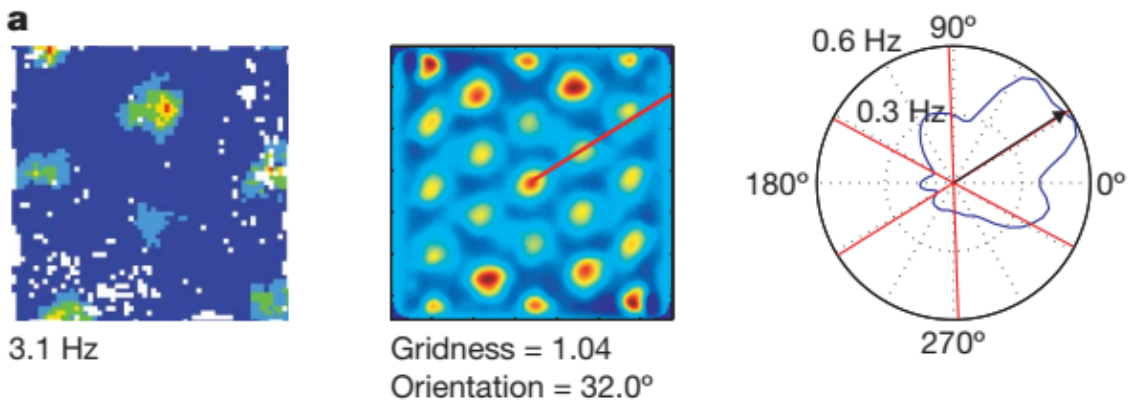


Figure 5: **The mean firing directions of directional grid cells are aligned with the grid.** Left panel shows the firing rate heat map for a ‘conjunctive’ directional grid cell (red, high firing rate; blue, low rate; white, unvisited location; peak rate 3.1 Hz). Middle panel shows the heat map’s spatial autocorrelogram. Right panel shows the polar firing rate map for the same cell, where the black arrow represents the mean firing direction, and red lines indicate the main axes of the grid firing pattern identified from the spatial autocorrelogram. Image:[9].

3 Methods

3.1 Data collection and fundamental methods

Data for 112 cell pairs was collected from rats moving freely in a one meter square environment (31 March 2006 to 16 May 2011). The video/computer methods used for location tracking are described in [1, Supp.] and in much earlier work, e.g. [20, 25].

Spike rate maps were created using the method developed by Muller *et al.* [23]. The environment was binned into 2x2 cm squares, the cell's firing rate was computed for each square, then these rates were smoothed with a boxcar algorithm in two dimensions to generate a heat map for each tetrode cell pair [1, Supp.].

All rate maps in this report use typical heat map colours where shades of red, yellow, green and blue indicate spike rates from high to low respectively.

3.2 Software

All software for this project was implemented using Matlab 2018b, various toolboxes, and functions defined in two specialised toolboxes in particular.

1. The Universal_Matlab (UM) toolbox [Barry Lab, UCL].
2. The CircStat toolbox for circular statistics by Philipp Berens [3].

All Matlab functions mentioned will be in this font: `function_name`.

3.3 Cell classification

Figure 6 provides a quick summary of border cells, grid cells, and HD cells. This report is primarily about cells with grid and direction properties. Two properties of interest are the cell's gridness and its Rayleigh vector (mean resultant vector). Both will be presented in more detail in the next sections.

Figure 6(a) shows a rate map for a border cell, and (b) shows a spatial auto-correlogram for a grid cell. Figure 6(c) shows a bimodal distribution of grid scores; the red line at 0.5 is the threshold for grid cells in this case, in contrast a subjective gridness threshold of 0.3 was used in [1]. Figure 6(e) shows a bimodal distribution

of Rayleigh vector lengths for cells recorded in the dorsal presubiculum, and the red line at 0.3 marks the threshold for HD cells.

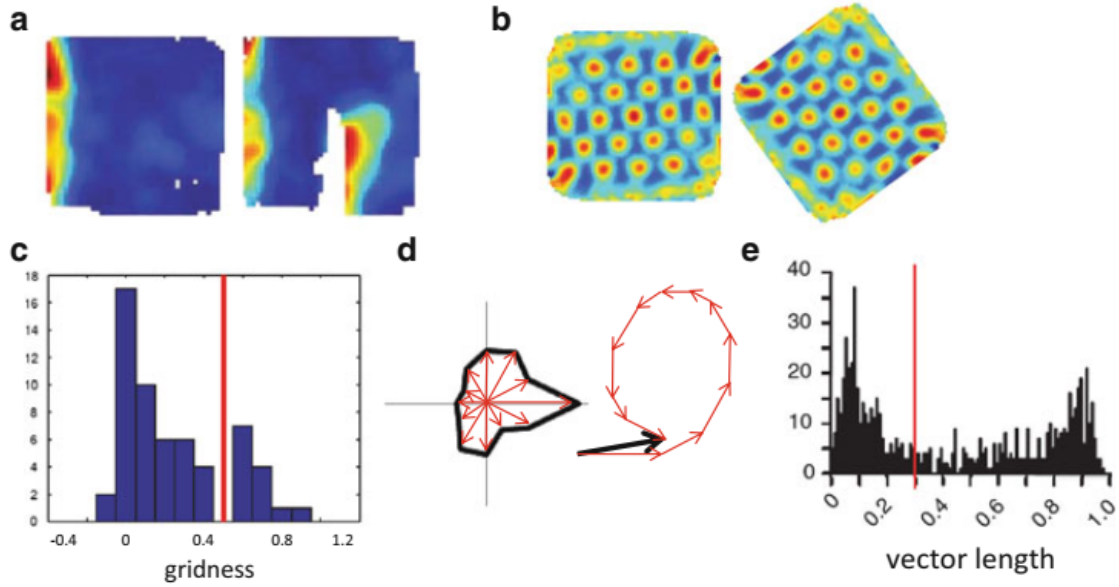


Figure 6: Cell type classification: (a) border cells fire near a border regardless of environment, (b) calculation of gridness is based on the spatial autocorrelation of the original spatial firing pattern with rotated versions, (c) typical distribution of gridness scores, (d) calculation of Rayleigh vector length, (e) distribution Rayleigh vector lengths for cells recorded in the dorsal presubiculum. Image:[8, p114].

3.4 Grid properties

I used the Universal Matlab functions `xPearson(smooth_rate_map)` to compute spatial autocorrelation (sac) of the rate map, and `multigridness(sac)` to compute the standard gridness score, same as in [13]. Gridness was computed using the method described in [1, Supp.] where cells with scores 0.3 or greater were classified as grid cells.

3.5 Centre of Mass

Figure 8(a) shows a spike rate map and its centre of mass (CoM) vector. The CoM for each spike rate map was calculated using the following Matlab script

```

x = 1:size(rate_map, 2); % Columns.
y = 1:size(rate_map, 1); % Rows.
[X, Y] = meshgrid(x, y);
mean_m = nanmean(M(:));
mean_x = nanmean(M(:) .* X(:)) / mean_m;
mean_y = nanmean(M(:) .* Y(:)) / mean_m;

```

Figure 7: The script for calculating the CoM.

where `rate_map` is a matrix and the Cartesian coordinate (`mean_x`, `mean_y`) is at the centre of the map.

3.6 Place by direction sampling bias correction (PxD)

If a neuron is directional, then in a small arena its firing will be spatially inhomogeneous [7, 22]. But not every head direction can be equally sampled in every location, and spikes will tend to accumulate at locations where the animal is able to look in the cell’s preferred HD. In this case, it is necessary to normalise spike rates [6].

To eliminate the effect of uneven directional sampling of directional cells, I used `pxd` to generate spike rate maps. The function `pxd` is based on the maximum likelihood factorial model (MLM) [6]; it provides an estimate of unbiased spatial firing. Figure 8(b) shows a spike rate map and its CoM vector after PxD correction.

3.7 Place Fields

Figure 8(c) shows the PxD corrected spike rate map for one cell recorded by tetrode 3 (from rat 214) after it was partitioned into seven place fields numbered 1 to 7 by the `fs_findFields` function. Watershed field boundaries are clearly delineated in Figure 8(d).

In this example, I projected the seven field centres onto the blue CoM axis line; the orthogonal projection points are represented by magenta stars. The mean projection point is marked by a white X, which is left of centre. The original CoM vector line is red and points left.

The field centres are the peak rate bins for each watershed field, and their mean projection point on the CoM axis is an unweighted mean of the projection points, which may indicate a shift of the entire grid as opposed to a locally weighted shift

of the CoM due to one or two fields with many spikes, which could imply that the grid is asymmetric and/or heterogeneous. For example, in Figure 8(c), the entire grid has shifted to the left and the large number of spikes in field 2 (bright yellow) has moved the CoM left and down. So, the grid for this cell is asymmetric and heterogeneous, i.e. very responsive to one particular place x HD combination.

21403101: t=3, c=1, spikes=379

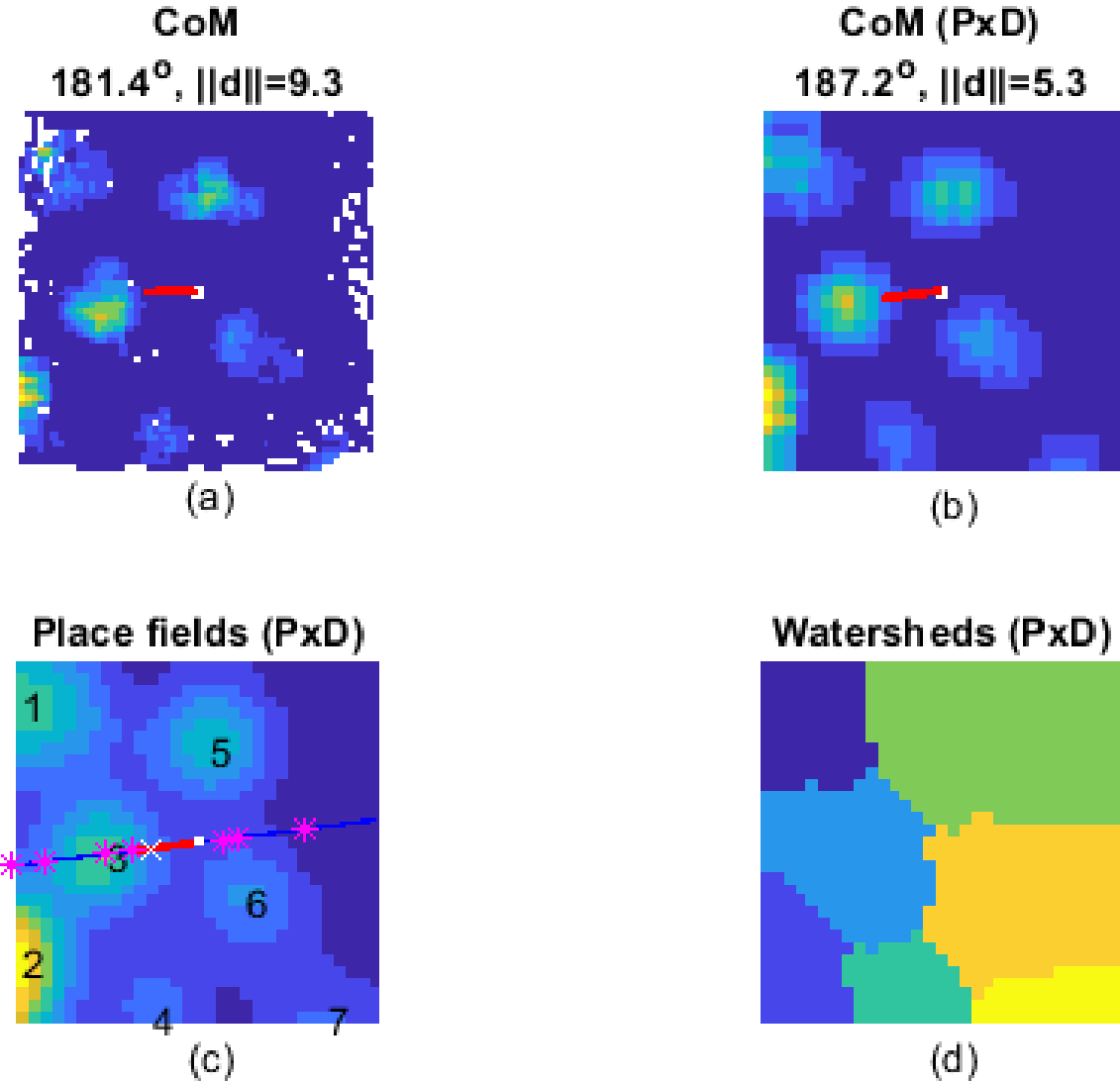


Figure 8: Example rate maps and place fields: (a) spike rate map with CoM vector, direction 181.4° and magnitude 9.3, (b) corrected spike rate map with CoM vector, direction 187.2° and magnitude 5.3, (c) place field map with numbered field centres projected onto the CoM axis (each marked by a magenta *), a white X marks the mean field centre projection point, and the small white square in the centre marks the origin. Note: maps (b), (c) and (d) were corrected for place by direction (Px D) sampling bias.

3.8 Head direction properties

I used the CircStats functions `circ_r` and `circ_mean` to compute the Rayleigh vectors. Conceptually, head direction properties can be computed from the polar head directions [19, 46], as shown in Figure 6(d).

HD cells typically display a Rayleigh vector length of at least ~ 0.25 (on a scale from 0 to 1). About 50% of the cells in the MEC meet this threshold [4], but the degree of directional tuning tends to be less in the MEC than in pre- and parasubiculum [8, p115].

3.8.1 Polarplots

Polarplots were generated with the script in Figure 9; functions `circ_r`, `circ_mean`, and `circ_rtest` are discussed in the follow sections.

```
smooth_dir = easy_make_polarplot( data, tet_idx, cell_num, exact_cut);
theta = (circshift(linspace(0,2*pi,60),30))'
polarplot(theta, smooth_dir)
d=(2*pi)/60                                % d: correction factor for binning
R=circ_r(theta, smooth_dir, d)
p=circ_rtest(smooth_dir)
rad=circ_mean(theta, smooth_dir, 'all')
polarplot([rad,rad], [0,r], 'Linewidth', 2)
```

Figure 9: The script for generating polar plots. All angles and directions are in radians.

3.8.2 The mean resultant vector

The length of the mean resultant vector is a measure of circular spread. The closer it is to one, the more concentrated the data sample is around the mean direction. The mean resultant vector was computed by $\bar{r} = \text{circ_mean}(\text{smooth_dir})$.

Vector length is defined by the equation

$$R = \|\bar{r}\| \tag{1}$$

and was computed by `R = circ_r(smooth_dir)`. The estimation of `R` is biased when binned data is used and can be corrected by supplying the bin spacing `d` as a

third argument and computing a correction factor [50, Equation 26.16]

$$c = \frac{d}{2 \sin(d/2)} \quad (2)$$

setting $R_c = cR$.

3.8.3 The Rayleigh test

The Rayleigh test asks how large the resultant vector length R must be to indicate a non-uniform distribution [24, 50]. This test is well suited for detecting a unimodal deviation from uniformity [3].

The Rayleigh test was performed by computing `p = circ_rtest(smooth_dir)` where a small p value indicates a significant departure from uniformity [3].

4 Results

4.1 Summary of all cells

Figure 10 is a data summary of all cells. These were corrected for place by direction sampling bias using the function `pxd`, based on [6]. The directional bias for the CoM and preferred HD vectors is in row 2 similar, as is the distribution of vector magnitudes in row 3. Figure 17 in the Appendix summarises the same data before PxD correction.

Table 1 presents a summary of gridness and directional statistics for all cells, both before and after PxD correction, which had large impact on some metrics of interest, i.e. mean gridness was reduced from 0.67 to 0.25, and CoM $\|d\|$ was reduced from 2.51 to 1.29. However, this may be correct. For example, the distribution of preferred HD vector lengths ($\|r\|$) in Figure 10 is similar to the distribution Rayleigh vector lengths in Figure 6(e). And although the threshold for HD cells is ~ 0.3 in that figure, compared to a mean length 0.16 for the cells in this report, cells in the presubiculum tend to be more directional than in the MEC [8, p115].

Figure 11 shows polar plots for the CoM vectors \vec{d} and the directional vectors (Rayleigh vectors) \vec{r} . As expected, the distribution of magnitudes is skewed to small values, while direction is more evenly spread over 360° .

Gridness and Direction (PxD), cell count 112

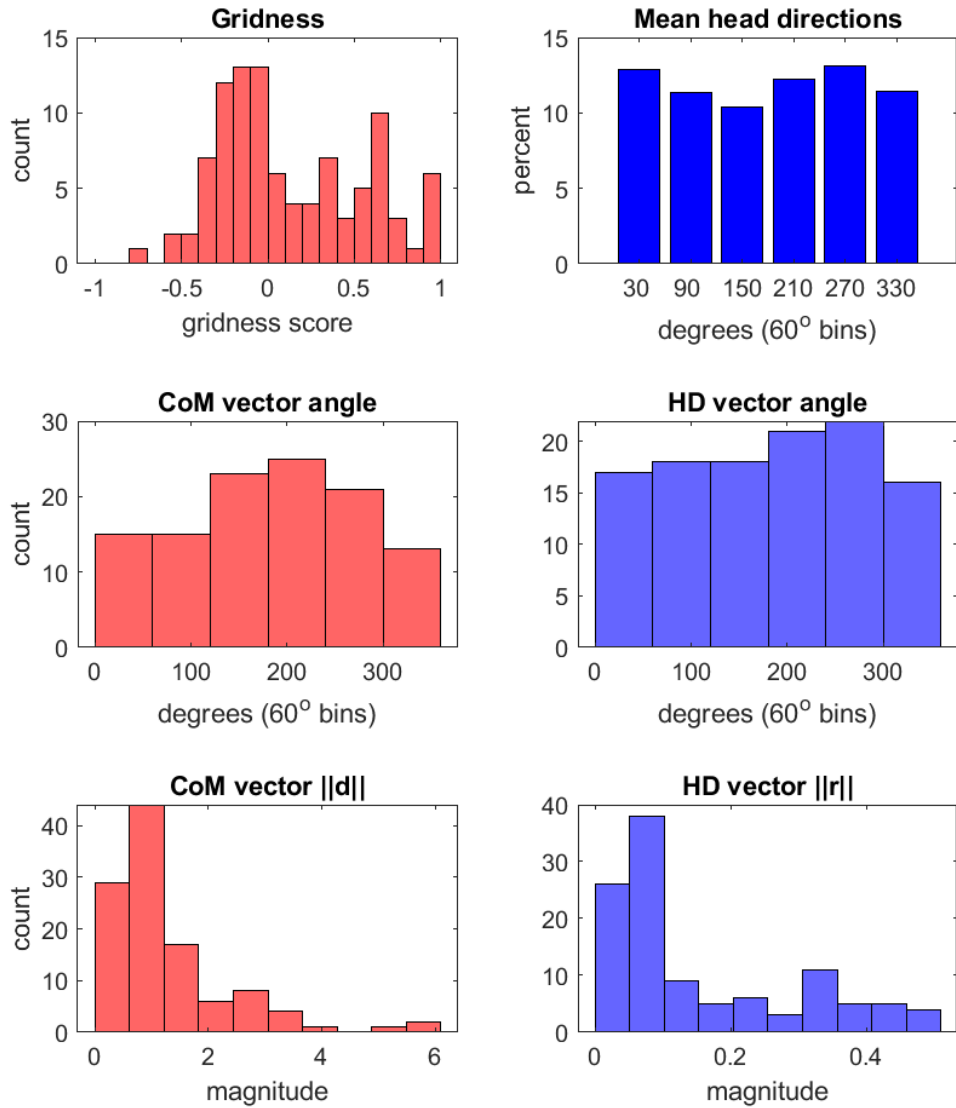


Figure 10: Histograms for gridness and direction (all cells), corrected for place by direction (PxD) sampling bias.

	mean	standard deviation	minimum	maximum
Gridness	0.67	0.49	-0.69	1.38
Gridness (Px D)	0.25	0.51	-0.72	1.33
CoM $\ d\ $	2.51	2.17	0.37	12.77
CoM $\ d\ $ (Px D)	1.29	1.11	0.07	6.10
HD $\ r\ $	0.16	0.13	0.00	0.46
HD $\ r\ $ (Px D)	0.16	0.14	0.01	0.50

Table 1: Summary statistics for all 112 cells.

CoM and HD vector angles (Px D), cell count=112

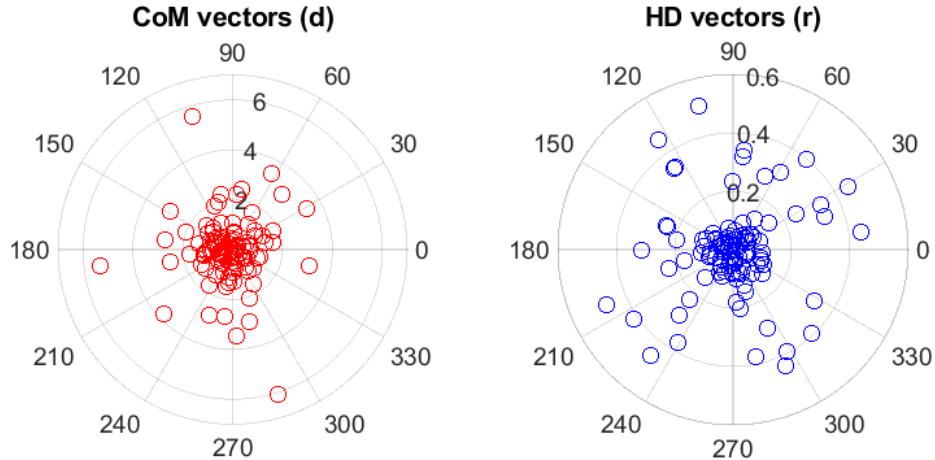


Figure 11: Polar plots for CoM and directional vector (all cells), after Px D correction.

4.2 Gridness and directionality depend on cell type

The place by direction corrected rate maps (pxd) should provide an unbiased estimate of the pure spatial and directional rate map. Figure 12 shows maps for one cell: an uncorrected rate maps (row 1), and corrected rate maps (row 2).

Uncorrected rate maps typically use about 2500 spatial bins ($\sim 4\text{cm}^2$) each, and 60 directional bins (6 degrees each). Corrected rate maps typically use about 625

spatial bins $\sim 16\text{cm}^2$ each and 360 directional bins (1 degree each).

The lower peak rate for row 2 is partly due to the larger bin size used by pxd. The pxd generated polar plot looks very different from the uncorrected version partly due to its 1 degree directional bins, and vector magnitude is slightly less for this cell.

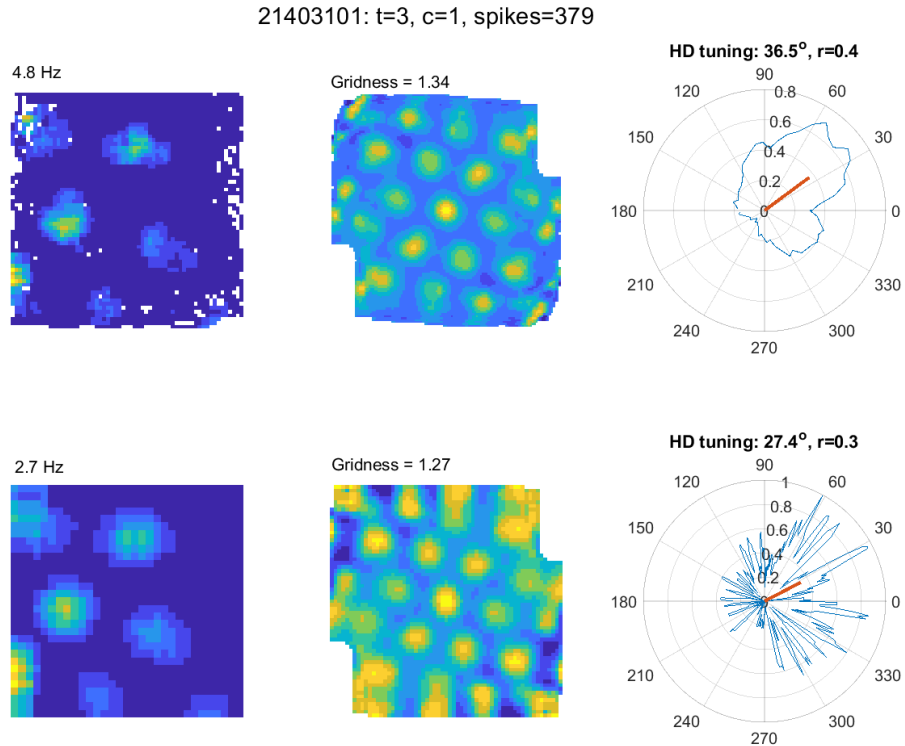
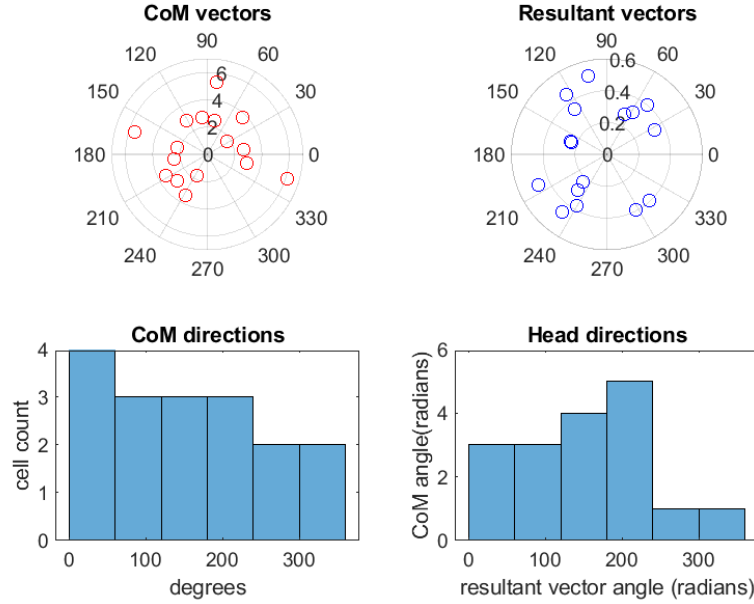


Figure 12: Rate maps: row 1 uncorrected, row 2 was corrected for PxD sampling bias.

4.3 CoM vector direction and the HD vector for some cells are correlated after PxD correction

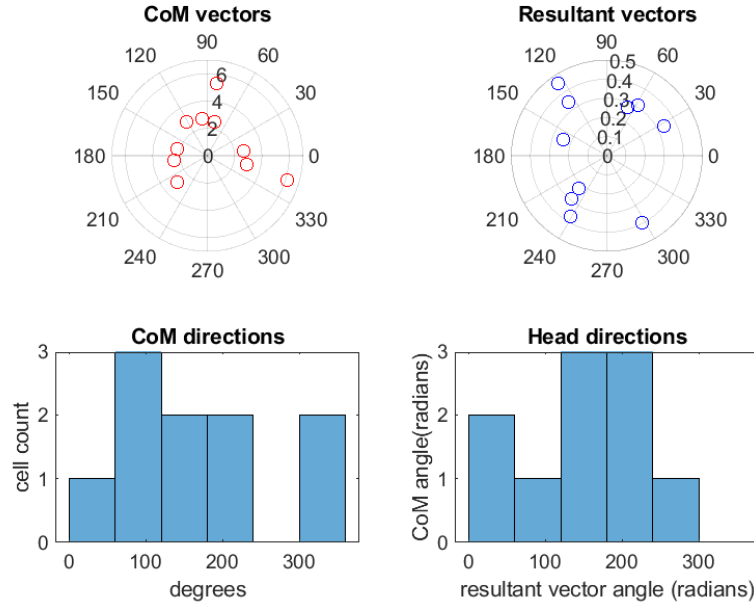
Figure 13 shows polar plots and histograms for the small number of cells that passed a set of three thresholds (T_g for gridness, T_d for $\|d\|$, and T_r for $\|r\|$). The application of higher thresholds greatly reduces the number of cells and tends to make statistically significant results less likely.

CoM v HD angles: cells=17, $T_g = -1.0$, $T_d = 1.40$, $T_r = 0.13$



(a) Thresholds: gridness ≥ -1.0 and $\|d\| \geq 1.40$ and $\|r\| \geq 0.13$.

CoM v HD angles: cells=10, $T_g = 0.2$, $T_d = 1.40$, $T_r = 0.13$



(b) Thresholds: gridness ≥ 0.2 and $\|d\| \geq 1.40$ and $\|r\| \geq 0.13$.

Figure 13: Useful thresholds can reduce the number of cells from 112 to less than 20: (a) Gridness ≥ -1.0 : 17 cells, (b) Gridness ≥ 0.2 : 10 cells. PxD corrected.

Gridness, $\|d\|$, and $\|r\|$ have an impact on the correlation of a cell's CoM direction with its preferred HD. To gain some insight into this relationship, these parameters were optimised as thresholds. Figure 14 shows the results where the optimisation algorithm evaluated combinations of thresholds to find the combination with the

highest positive correlation on the condition that the associated p-value was ≤ 0.05 and included at least 10 cells. Significant negative correlation occurred with some threshold combinations, but those results have been omitted for clarity.

Figure 14(a) shows the bar chart for correlation of the CoM vectors with preferred HD vectors after PxD correction. Given optimal thresholds for $\|d\|$ and $\|r\|$, statistically significant correlation is only present when cells with low gridness are included, i.e. when the gridness threshold is not greater than -0.5.

It may be worth noting that the results reported in this section are very different from what was observed when using data that was not PxD corrected, i.e. Figure 19 in the Appendix shows that correlation also occurred in the gridness threshold range of about 0.25 to 0.65, and was maximised when a gridness threshold of ≥ 0.5 was applied.

In Figure 14(b) below, correlation exists only in a narrow range of CoM vector $\|d\|$ thresholds, given optimal thresholds for $\|r\|$ (0.14) and gridness (-1.0). In Figure 14(c), correlation exists over a range of low $\|r\|$ thresholds, given optimal thresholds for $\|d\|$ and gridness.

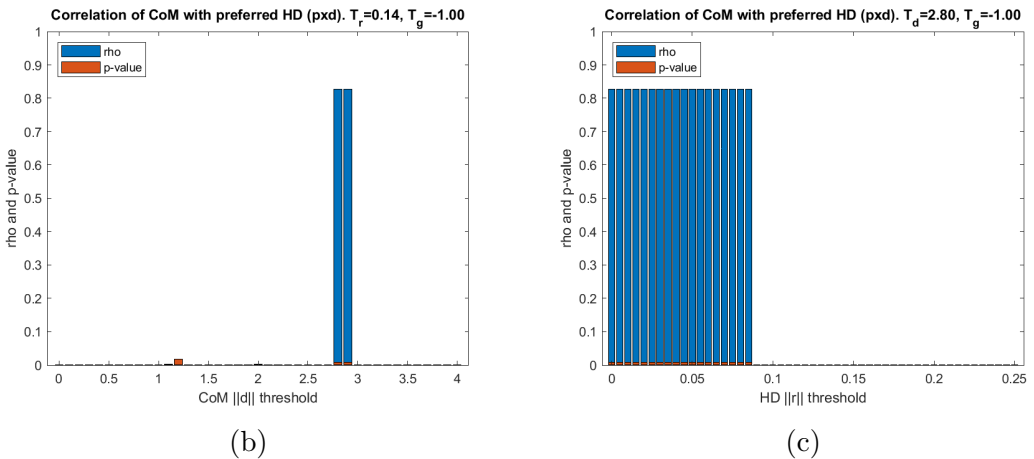
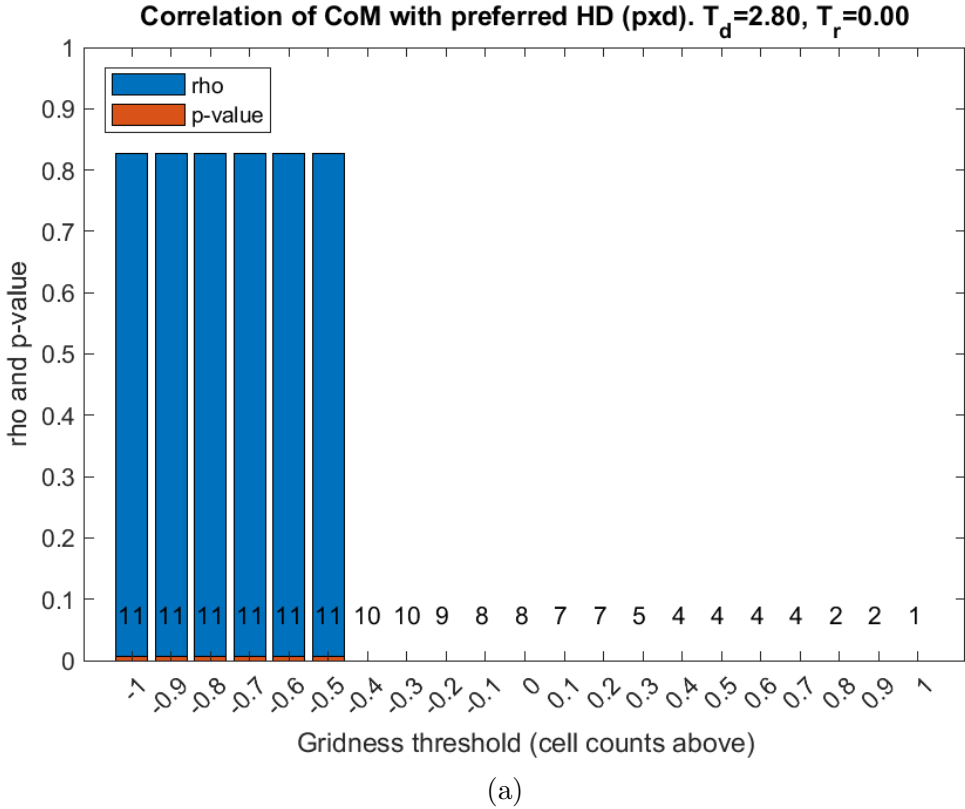


Figure 14: Correlation of CoM direction with preferred head direction optimised for maximum correlation: (a) p -values ≤ 0.05 shown in red, p -values > 0.05 were set to 0, correlation with p -values ≤ 0.05 and at least 10 cells shown in blue, insignificant correlation values were set to zero, (b) significant correlation exists in a narrow range of CoM $\|d\|$ thresholds given optimal thresholds for $\|r\|$ and gridness, (c) significant correlation exists for range of small $\|r\|$ thresholds (well below the mean $\|r\|$ of 0.16), given optimal thresholds for $\|d\|$ and gridness.

Figure 15 shows the correlation of CoM direction with preferred head direction after the thresholds were optimised for the highest mean correlation over the independent domain (as opposed to a single maximum correlation). In Figure 15(a) the significant correlation exists at opposite ends of the gridness threshold domain

bimodal.

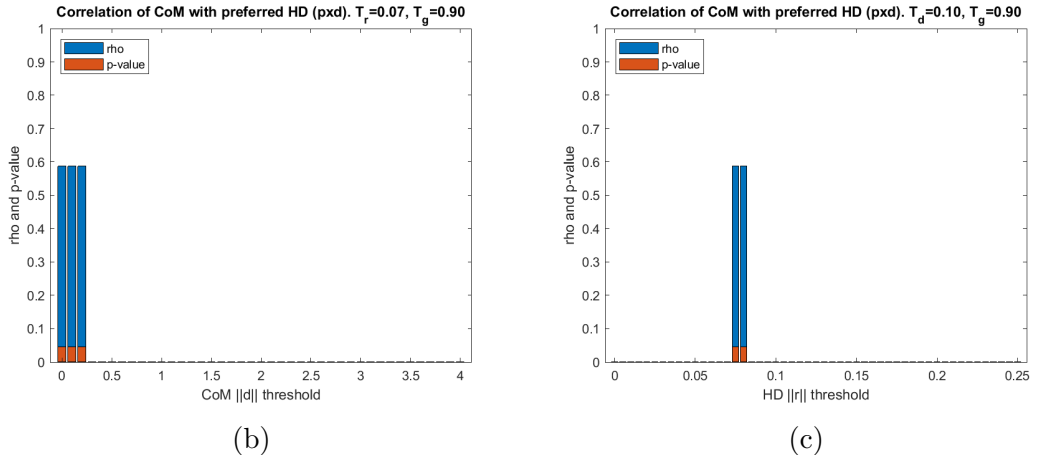
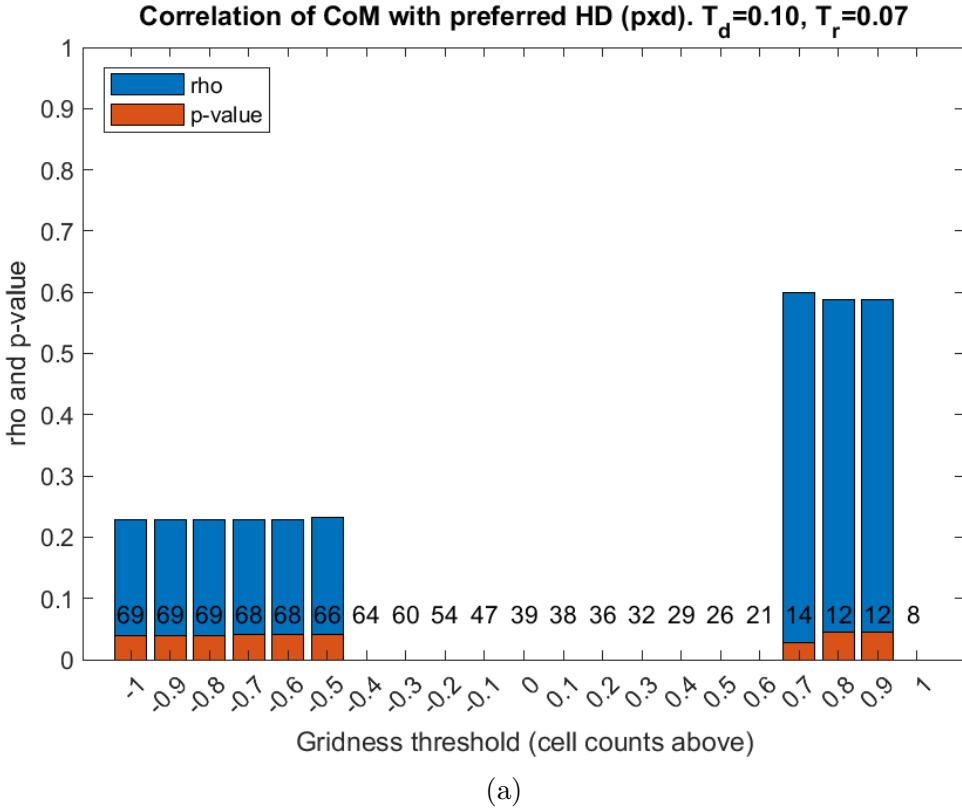


Figure 15: Correlation of CoM direction with preferred head direction optimised for the highest mean correlation over the independent domain: (a) correlation is bimodal given optimal thresholds for $\|d\|$ and $\|r\|$, (b) correlation exists for small $\|d\|$ thresholds, given the optimal threshold for $\|r\|$ and gridness, (c) a narrow range of $\|r\|$ thresholds is associated with correlation given the optimal thresholds for $\|d\|$ and gridness.

4.4 Place fields and grid shifts

Figure 16 shows rate maps and place fields for an example cell. Figure 16(a) shows its CoM vector in red and (b) shows the boundaries of each watershed field, but

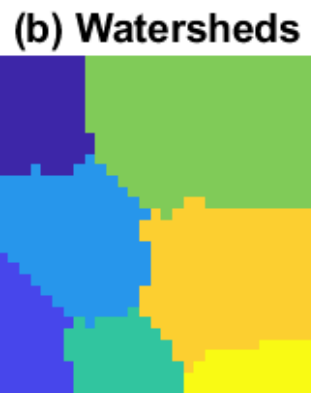
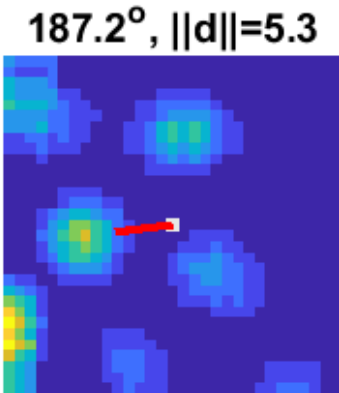
what caused the CoM to move? Did the entire grid shift, or is the magnitude and direction of this vector due to a small number of fields with high spike counts? In other words, was the shift caused by global or local factors?

In Figure 16(c), the seven peak rate field centres were projected onto the CoM axis. In this case, field spike count had no impact on the projection points, and the mean projection point indicated a global grid shift of 4.15.

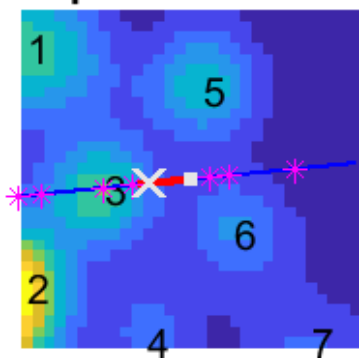
In Figure 16(d), the seven CoM field centres were projected onto the CoM axis. In this case, field spike counts weighted the projection points, and the mean projection point indicated a spike weighted local grid shift of 3.24.

21403101: t=3, c=1, spikes=379

(a) Grid with CoM (PxD)



(c) Place fields with peak rate centres



(d) Place fields with CoM centres

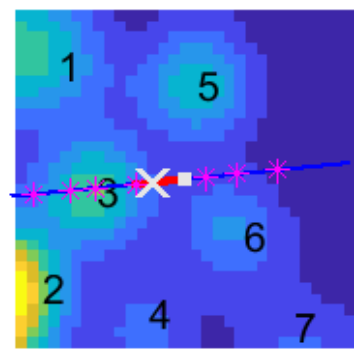


Figure 16: Place fields and grid shifts: (a) PxD corrected rate map with CoM vector, $\|d\| = 5.3$ from the origin (white square) to the CoM, (b) place fields delineated by the watershed algorithm; in (c) and (d) the numbered place fields have been projected onto the CoM axis, the white X marks the mean projection point for the peak rate field centres, grid shift=4.15, (d) numbered place fields with CoM centres projected onto the CoM axis, the white X indicates the mean projection point, grid shift=3.24. Rate maps were corrected for PxD sampling bias.

In following tables low gridness is associated with highly variable field and grid properties. Table 2 shows field statistics and Table 3 shows global and local grid shift statistics for a total of 253 fields in 49 cells with above average gridness, i.e. ≥ 0.25 .

Table 4 shows field statistics and Table 5 shows global and local grid shift statistics for a total of 243 fields in 63 cells with below average gridness, i.e. < 0.25 .

	mean	standard deviation	minimum	maximum
Per bin (Hz)	1.06	0.29	0.57	1.68
Per field (Hz)	118.24	133.41	1.24	982.70
Field area (bins)	120.6	80.45	3	421

Table 2: Field statistics for cells with gridness ≥ 0.25 . Cell count 49, field count 253.

	mean	standard deviation	minimum	maximum
Global grid shift	1.94	1.70	0.05	8.84
Local grid shift	1.62	1.25	0.001	5.02

Table 3: Gridness ≥ 0.25 : global versus local shifts along the CoM axis. Cell count 49, field count 253.

	mean	standard deviation	minimum	maximum
Per bin (Hz)	1.32	0.31	0.67	1.87
Per field (Hz)	267.57	927.70	1.00	7972.81
Field area (bins)	152.5	140.57	3.00	676.00

Table 4: Field statistics for cells with gridness < 0.25 . Cell count 63, field count 243.

	mean	standard deviation	minimum	maximum
Global grid shift	2.70	2.05	0.15	11.58
Local grid shift	1.88	1.51	0	5.69

Table 5: Gridness < 0.25 : global versus local shifts along the CoM axis. Cell count 63, field count 243.

5 Discussion

The spatial map in the MEC comprises both grid cells and head-direction cells. These cell types do not form discrete populations, rather they form a continuous population. Grid cells express variable degrees of directional modulation and head-direction cells express variable degrees of grid structure [35]. The conclusion by Sargolini *et al.* [35] seems to be consistent with the results presented in this report.

After PxD correction, imposing higher and higher gridness thresholds did not increase the correlation of the CoM vector \vec{d} with the preferred HD vector \vec{r} . Quite the opposite. Considering Figure 14, correlation was highest when the gridness threshold was in the -1 to -0.5 range, and not significant at gridness thresholds ≥ -0.5 . This result is somewhat intuitive. “Pure” grid cells, such as those with high gridness scores, are mostly or perhaps exclusively responsive to place. Cells with less gridness can afford to be responsive to direction and place. For directional correlation of CoM with preferred HD, it seems that no gridness is required.

Figure 15(a) was based a different optimisation. Thresholds were found that maximised the mean correlation over the entire domain. The gridness range from -1 to -0.5 was once again associated with positive correlation for about 68 cells, but a small set of cells with high gridness scores (thresholds from 0.7 to 0.9) were associated with higher levels of correlation. So, perhaps this subset of just 14 cells are the real conjunctive grid cells.

The statistics in Tables 2 to 5 for place fields and grid shifts, as illustrated by Figure 16, indicate that fields are quite variable, and the magnitude of the CoM vector is mostly due to a global shift of the grid. Both factors contribute to grid asymmetry.

Tables 2 and 4 contain statistics about the place fields in cells with gridness of ≥ 0.25 and < 0.25 respectively. Standard deviation is consistently higher for the subset of cells with low gridness. This was expected because low gridness implies a firing topography with less structure and regularity.

Tables 3 and 5 contain statistics about the grids in cells with gridness of ≥ 0.25 and < 0.25 respectively. Using a gridness threshold of ≥ 0.25 , the mean global shift for these cells was 1.94 versus 1.62 for the local shift ... a relatively small difference. However, using a gridness threshold of < 0.25 , the mean global shift for these cells was 2.70 versus 1.88 for the local shift. This consistent result suggests that, in

general, global grid shifts contribute more to CoM vector magnitude $\|d\|$ and have a bigger impact on grid asymmetry than local grid shifts. This is especially true for cells with low gridness.

Whether or not global versus local shifts are relevant to the correlation between a cell's CoM vector direction and its preferred HD is not yet clear from the data analysis in this report.

6 Future Work

The results based on the PxD corrected rate maps were not as expected. It may be that there is an error in my Matlab code, or that the `pxd` function was not applied correctly at some point. In any event, perhaps with more cells the functional interaction between parameters will result in a smoother output as opposed to the very discontinuous output often seen in this report.

The current version of Universal_Matlab builds rate maps that mix place spikes with directional spikes. It should be possible to build two maps, one for spikes closely associated with preferred direction, and the other built from spikes recorded while the animal was not facing in the cell's preferred HD.

Place fields and grid shifts, as illustrated by Figure 16, could shed more light on conjunctive grid cells and the interaction of place tuning versus directional tuning. It may be that each field is directional in some cells and that each field's directional tuning is correlated with the cell's mean resultant vector which is based on the entire rate map.

Instead of just more data analysis, it might be interesting to also apply some pharmacological methods. For example, in vivo recordings combined with neural manipulations have been used to examine interdependence and coherence between HD cell, grid cell, and place cell activity. In general, perturb one type of spatially tuned signal by manipulating activity in a circuit node and, at the same time, record a different spatially tuned signal at another location in the circuit. Results by Winter et al. [47] suggested that the HD signal is necessary for the generation of grid cell activity.

References

- [1] Caswell Barry, Robin Hayman, Neil Burgess, and Kathryn J Jeffery. Experience-dependent rescaling of entorhinal grids. *Nature neuroscience*, 10:682–684, June 2007.
- [2] Caswell Barry, Colin Lever, Robin Hayman, Tom Hartley, Stephen Burton, John O’Keefe, Kate Jeffery, and Neil Burgess. The boundary vector cell model of place cell firing and spatial memory. *Reviews in the neurosciences*, 17:71–97, 2006.
- [3] Philipp Berens et al. Circstat: a matlab toolbox for circular statistics. *J Stat Softw*, 31(10):1–21, 2009.
- [4] Charlotte N Boccara, Francesca Sargolini, Veslemøy Hult Thoresen, Trygve Solstad, Menno P Witter, Edvard I Moser, and May-Britt Moser. Grid cells in pre- and parasubiculum. *Nature neuroscience*, 13:987–994, August 2010.
- [5] Vegard Heimly Brun, Trygve Solstad, Kirsten Brun Kjelstrup, Marianne Fyhn, Menno P Witter, Edvard I Moser, and May-Britt Moser. Progressive increase in grid scale from dorsal to ventral medial entorhinal cortex. *Hippocampus*, 18:1200–1212, 2008.
- [6] Neil Burgess, Francesca Cacucci, Colin Lever, and John O’Keefe. Characterizing multiple independent behavioral correlates of cell firing in freely moving animals. *Hippocampus*, 15:149–153, 2005.
- [7] Francesca Cacucci, Colin Lever, Thomas J Wills, Neil Burgess, and John O’Keefe. Theta-modulated place-by-direction cells in the hippocampal formation in the rat. *The Journal of neuroscience : the official journal of the Society for Neuroscience*, 24:8265–8277, September 2004.
- [8] Moser E.I. Derdikman D. *Space, Time and Memory in the Hippocampal Formation*, chapter Spatial Maps in the Entorhinal Cortex and Adjacent Structures., pages 107–125. Springer, Vienna, 2014.
- [9] Christian F Doeller, Caswell Barry, and Neil Burgess. Evidence for grid cells in a human memory network. *Nature*, 463(7281):657, 2010.

- [10] Marianne Fyhn, Torkel Hafting, Alessandro Treves, May-Britt Moser, and Edvard I Moser. Hippocampal remapping and grid realignment in entorhinal cortex. *Nature*, 446:190–194, March 2007.
- [11] Marianne Fyhn, Torkel Hafting, Menno P Witter, Edvard I Moser, and May-Britt Moser. Grid cells in mice. *Hippocampus*, 18:1230–1238, 2008.
- [12] Marianne Fyhn, Sturla Molden, Menno P Witter, Edvard I Moser, and May-Britt Moser. Spatial representation in the entorhinal cortex. *Science (New York, N.Y.)*, 305:1258–1264, August 2004.
- [13] Torkel Hafting, Marianne Fyhn, Sturla Molden, May-Britt Moser, and Edvard I Moser. Microstructure of a spatial map in the entorhinal cortex. *Nature*, 436:801–806, August 2005.
- [14] Eric L Hargreaves, Geeta Rao, Inah Lee, and James J Knierim. Major dissociation between medial and lateral entorhinal input to dorsal hippocampus. *science*, 308(5729):1792–1794, 2005.
- [15] Joshua Jacobs, Christoph T Weidemann, Jonathan F Miller, Alec Solway, John F Burke, Xue-Xin Wei, Nanthia Suthana, Michael R Sperling, Ashwini D Sharan, Itzhak Fried, and Michael J Kahana. Direct recordings of grid-like neuronal activity in human spatial navigation. *Nature neuroscience*, 16:1188–1190, September 2013.
- [16] Nathaniel J Killian, Michael J Jutras, and Elizabeth A Buffalo. A map of visual space in the primate entorhinal cortex. *Nature*, 491:761–764, November 2012.
- [17] Emilio Kropff, James E Carmichael, May-Britt Moser, and Edvard I Moser. Speed cells in the medial entorhinal cortex. *Nature*, 523:419–424, July 2015.
- [18] Lukas Kunz, Tobias Navarro Schröder, Hweeling Lee, Christian Montag, Bernd Lachmann, Rayna Sariyska, Martin Reuter, Rüdiger Stirnberg, Tony Stöcker, Paul Christian Messing-Floeter, Juergen Fell, Christian F Doeller, and Nikolai Axmacher. Reduced grid-cell-like representations in adults at genetic risk for alzheimer’s disease. *Science (New York, N.Y.)*, 350:430–433, October 2015.
- [19] Rosamund F Langston, James A Ainge, Jonathan J Couey, Cathrin B Canto, Tale L Bjerknes, Menno P Witter, Edvard I Moser, and May-Britt Moser.

Development of the spatial representation system in the rat. *Science (New York, N.Y.)*, 328:1576–1580, June 2010.

- [20] BL McNaughton, Carol A Barnes, and J O’keefe. The contributions of position, direction, and velocity to single unit activity in the hippocampus of freely-moving rats. *Experimental brain research*, 52(1):41–49, 1983.
- [21] Bruce L McNaughton, Francesco P Battaglia, Ole Jensen, Edvard I Moser, and May-Britt Moser. Path integration and the neural basis of the’cognitive map’. *Nature Reviews Neuroscience*, 7(8):663, 2006.
- [22] R U Muller, E Bostock, J S Taube, and J L Kubie. On the directional firing properties of hippocampal place cells. *The Journal of neuroscience : the official journal of the Society for Neuroscience*, 14:7235–7251, December 1994.
- [23] R U Muller, J L Kubie, and J B Ranck. Spatial firing patterns of hippocampal complex-spike cells in a fixed environment. *The Journal of neuroscience : the official journal of the Society for Neuroscience*, 7:1935–1950, July 1987.
- [24] Fisher N.I. *Statistical Analysis of Circular Data*. Cambridge University Press, revised edition edition, 1995.
- [25] J O’Keefe. Spatial memory within and without the hippocampal system neurobiology of the hippocampus ed w seifert, 1984.
- [26] J O’Keefe and J Dostrovsky. The hippocampus as a spatial map. preliminary evidence from unit activity in the freely-moving rat. *Brain research*, 34:171–175, November 1971.
- [27] John O’keefe and Lynn Nadel. *The hippocampus as a cognitive map*. Oxford: Clarendon Press, 1978.
- [28] Carole Parron and Etienne Save. Evidence for entorhinal and parietal cortices involvement in path integration in the rat. *Experimental brain research*, 159:349–359, December 2004.
- [29] G J Quirk, R U Muller, J L Kubie, and J B Ranck. The positional firing properties of medial entorhinal neurons: description and comparison with hippocampal place cells. *The Journal of neuroscience : the official journal of the Society for Neuroscience*, 12:1945–1963, May 1992.

- [30] James B. Ranck. Head direction cells in the deep layer of dorsal presubiculum in freely moving rats. *Soc Neurosci Abstr*, 1984.
- [31] James B Ranck. Head direction cells in the deep cell layer of dorsolateral presubiculum in freely moving rats. *Electrical activity of the archicortex*, 1985.
- [32] A D Redish and D S Touretzky. Cognitive maps beyond the hippocampus. *Hippocampus*, 7:15–35, 1997.
- [33] A David Redish et al. *Beyond the cognitive map: from place cells to episodic memory*. MIT press, 1999.
- [34] David C Rowland, Yasser Roudi, May-Britt Moser, and Edvard I Moser. Ten years of grid cells. *Annual review of neuroscience*, 39:19–40, July 2016.
- [35] Francesca Sargolini, Marianne Fyhn, Torkel Hafting, Bruce L McNaughton, Menno P Witter, May-Britt Moser, and Edvard I Moser. Conjunctive representation of position, direction, and velocity in entorhinal cortex. *Science (New York, N.Y.)*, 312:758–762, May 2006.
- [36] Takuya Sasaki, Stefan Leutgeb, and Jill K Leutgeb. Spatial and memory circuits in the medial entorhinal cortex. *Current opinion in neurobiology*, 32:16–23, June 2015.
- [37] Patricia E Sharp. Complimentary roles for hippocampal versus subiculum/entorhinal place cells in coding place, context, and events. *Hippocampus*, 9(4):432–443, 1999.
- [38] Trygve Solstad, Charlotte N Boccara, Emilio Kropff, May-Britt Moser, and Edvard I Moser. Representation of geometric borders in the entorhinal cortex. *Science (New York, N.Y.)*, 322:1865–1868, December 2008.
- [39] Hanne Stensola, Tor Stensola, Trygve Solstad, Kristian Frøland, May-Britt Moser, and Edvard I Moser. The entorhinal grid map is discretized. *Nature*, 492:72–78, December 2012.
- [40] J S Taube and R U Muller. Comparisons of head direction cell activity in the postsubiculum and anterior thalamus of freely moving rats. *Hippocampus*, 8:87–108, 1998.

- [41] J S Taube, R U Muller, and J B Ranck. Head-direction cells recorded from the postsubiculum in freely moving rats. i. description and quantitative analysis. *The Journal of neuroscience : the official journal of the Society for Neuroscience*, 10:420–435, February 1990.
- [42] J S Taube, R U Muller, and J B Ranck. Head-direction cells recorded from the postsubiculum in freely moving rats. ii. effects of environmental manipulations. *The Journal of neuroscience : the official journal of the Society for Neuroscience*, 10:436–447, February 1990.
- [43] Jeffrey S Taube. Head direction cells recorded in the anterior thalamic nuclei of freely moving rats. *Journal of Neuroscience*, 15(1):70–86, 1995.
- [44] Jeffrey S. Taube. The head direction signal: origins and sensory-motor integration. *Annual review of neuroscience*, 30:181–207, 2007.
- [45] Sidney I Wiener and Jeffrey S Taube. *Head direction cells and the neural mechanisms of spatial orientation*. MIT Press, 2005.
- [46] Tom J Wills, Francesca Cacucci, Neil Burgess, and John O’Keefe. Development of the hippocampal cognitive map in preweanling rats. *Science (New York, N.Y.)*, 328:1573–1576, June 2010.
- [47] Shawn S Winter, Benjamin J Clark, and Jeffrey S Taube. Spatial navigation. disruption of the head direction cell network impairs the parahippocampal grid cell signal. *Science (New York, N.Y.)*, 347:870–874, February 2015.
- [48] Michael M Yartsev, Menno P Witter, and Nachum Ulanovsky. Grid cells without theta oscillations in the entorhinal cortex of bats. *Nature*, 479:103–107, November 2011.
- [49] Michael A Yassa and Craig E L Stark. Pattern separation in the hippocampus. *Trends in neurosciences*, 34:515–525, October 2011.
- [50] Jerrold H. Zar. *Biostatistical Analysis (5th Edition)*. Prentice-Hall, Inc., Upper Saddle River, NJ, USA, 2007.

7 Appendix

7.1 Summary

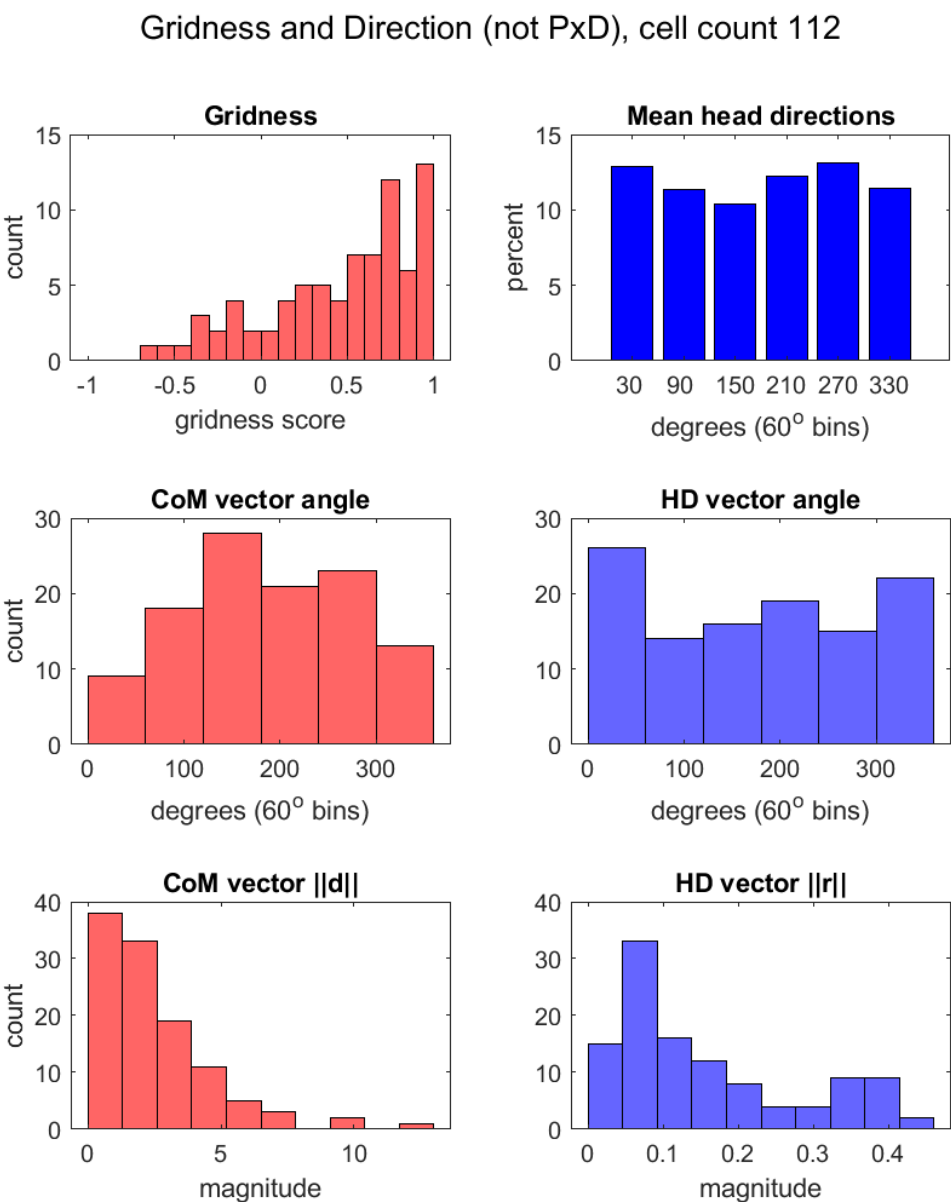


Figure 17: Histograms for gridness and direction (all cells), not PxD corrected for place by direction sampling bias.

CoM and HD vector angles (not PxD), cell count=112

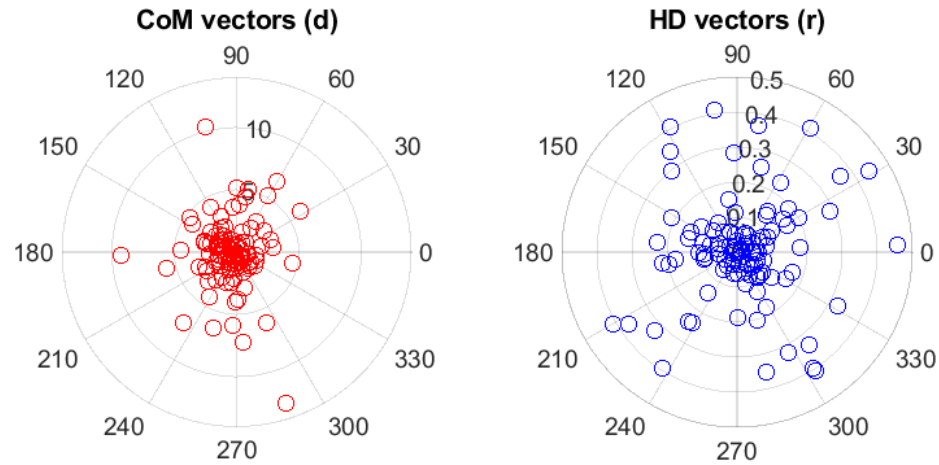


Figure 18: Polar plots for CoM and head direction (all cells), not PxD corrected.

7.2 Correlation

In Figure 19, gridness thresholds from 0.3 to 0.6 resulted in high correlation given optimal thresholds for $\|d\|$ and $\|r\|$ (without PxD correction).

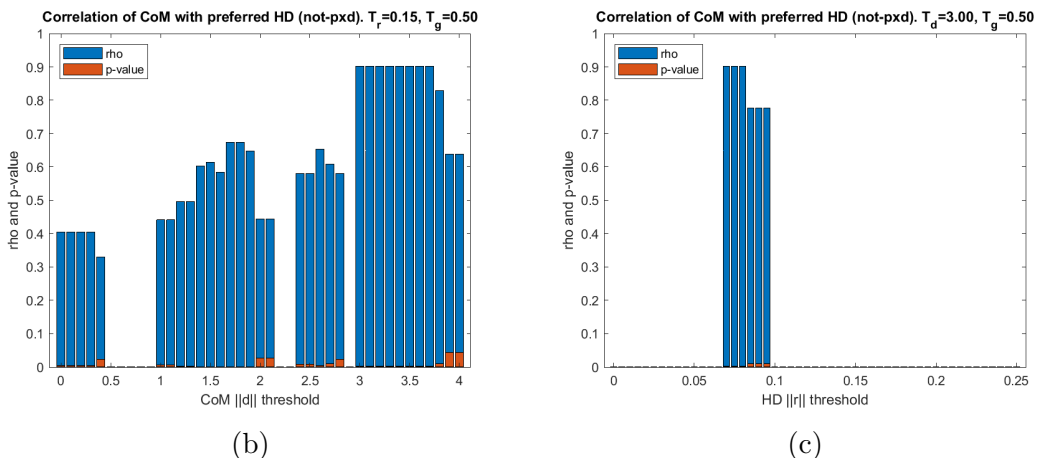
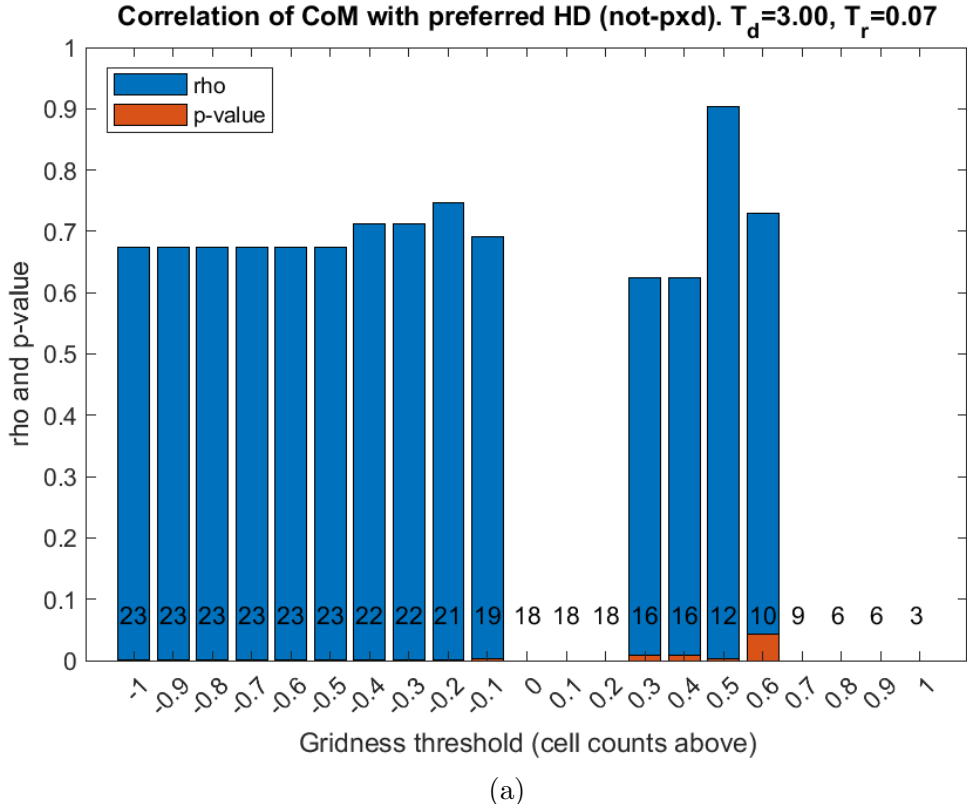


Figure 19: Correlation of CoM direction with preferred head direction using data that was not corrected for PxD sampling bias: (a) p-values ≤ 0.05 shown in red, correlation shown in blue, p-values > 0.05 were set to zero, correlation with p-values > 0.05 or less than 10 cells were set to zero, (b) correlation tended to increase with the magnitude of the CoM vector \vec{d} given optimal thresholds for HD tuning $\|r\|$ and gridness T_g , (c) significant correlation in a narrow middle range of HD tuning $\|r\|$ thresholds exists given optimal thresholds for CoM $\|d\|$ and gridness T_g .

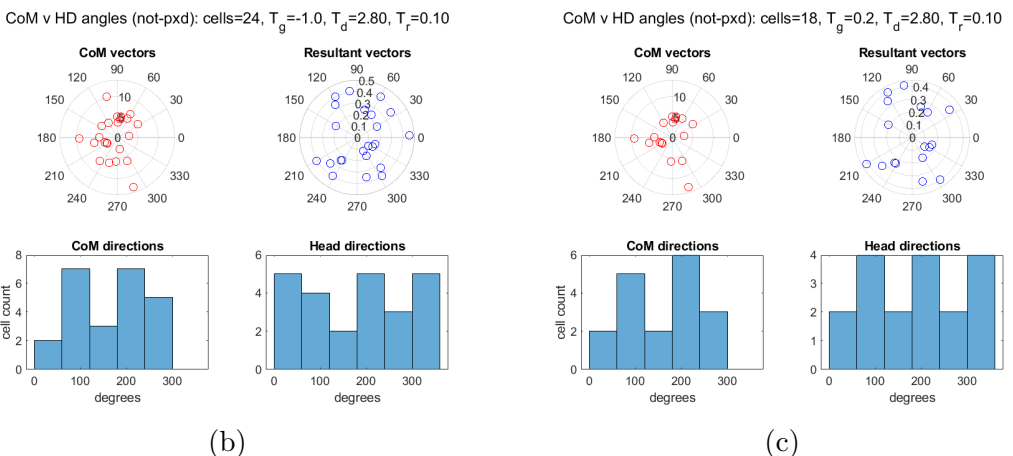
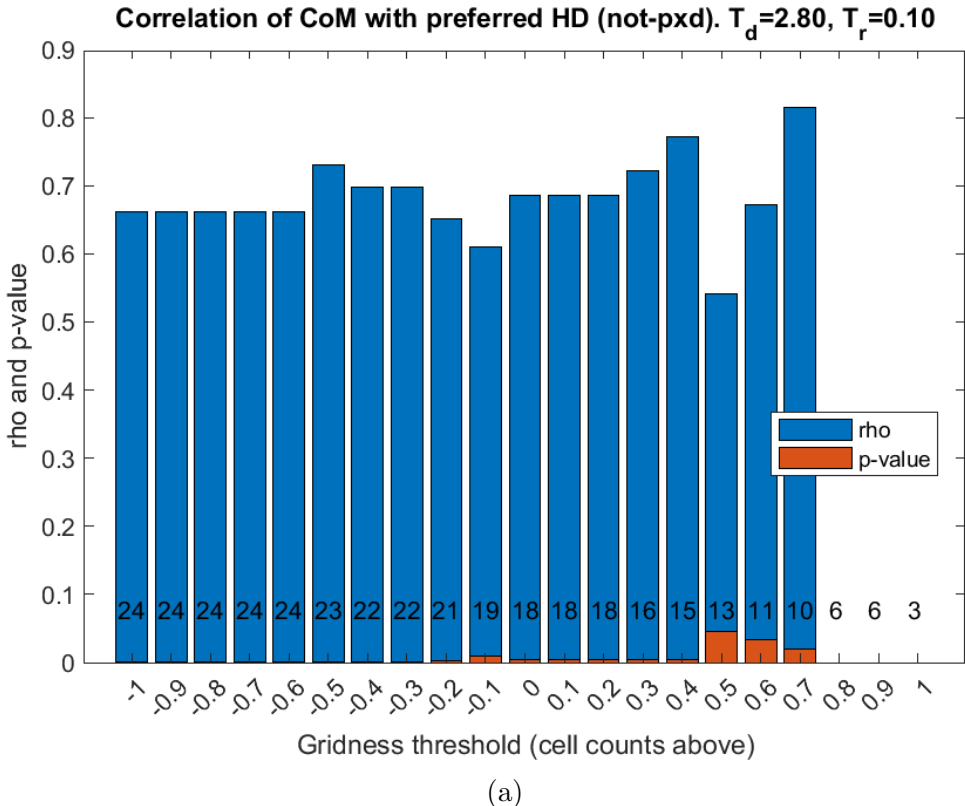


Figure 20: Non-optimal thresholds, using not PxD corrected rate maps.

7.3 Spike rate, spatial autocorrelation, and polar plots

Figures 21 to 34 show uncorrected maps in row 1 and PxD corrected maps in row 2 for the 12 cells with gridness ≥ 0.30 and directionality $\|r\| \geq 0.30$. However these threshold were applied to maps that were not PxD corrected (which tends to decrease gridness scores and the grid's peak firing rate per bin).

Spike rate maps are in column 1, spatial autocorrelograms in column 2, and polar plots in column 3 of each figure.

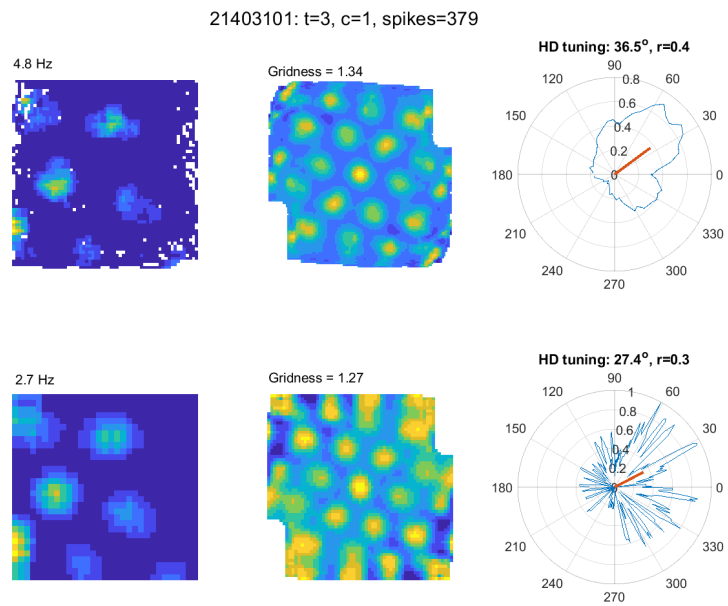


Figure 21

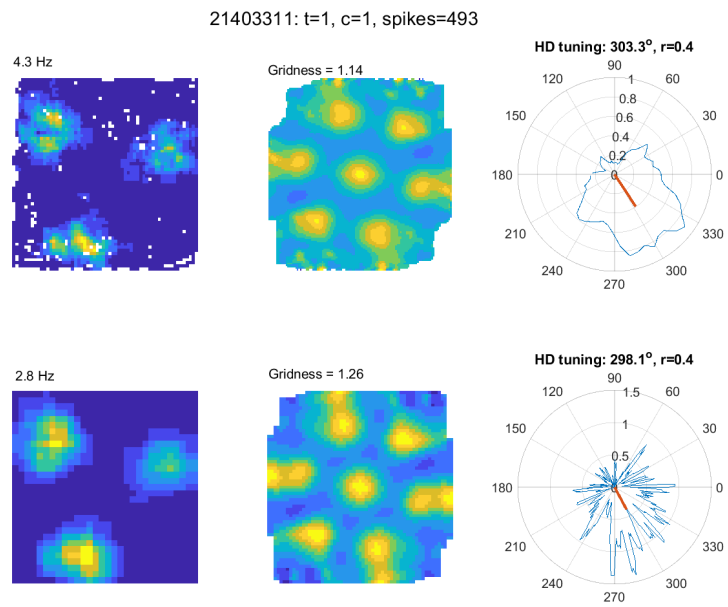


Figure 22

21404042: t=1, c=5, spikes=739

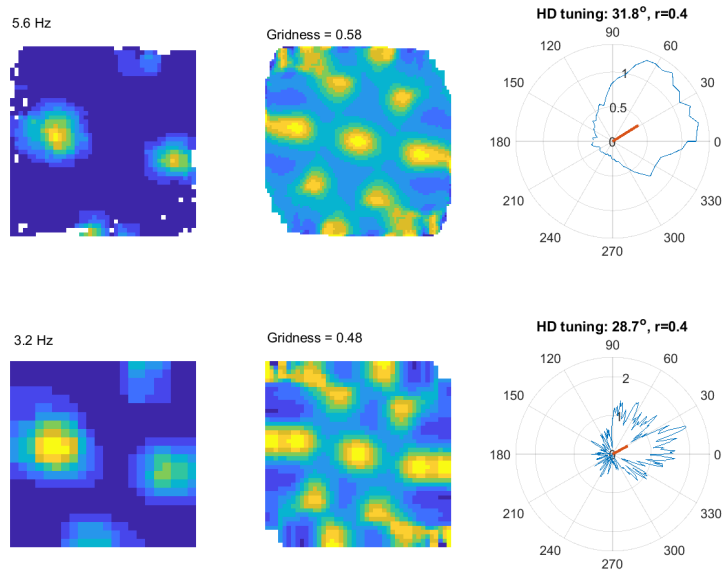


Figure 23

21605241: t=4, c=3, spikes=255

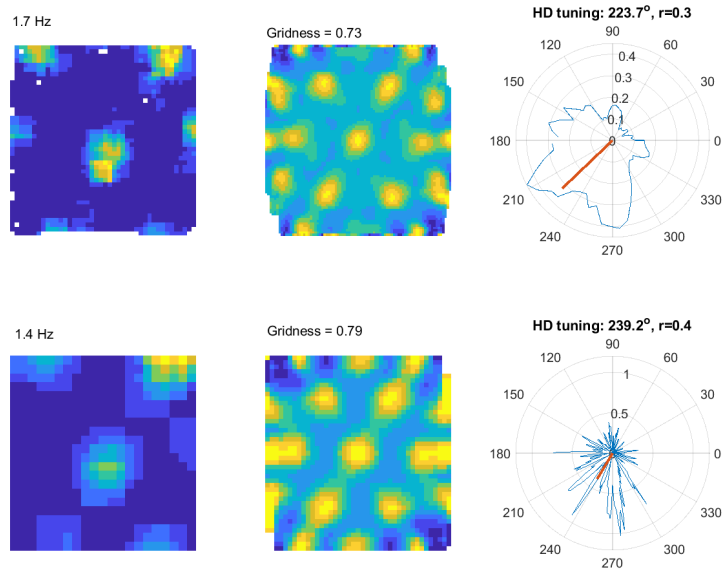


Figure 24

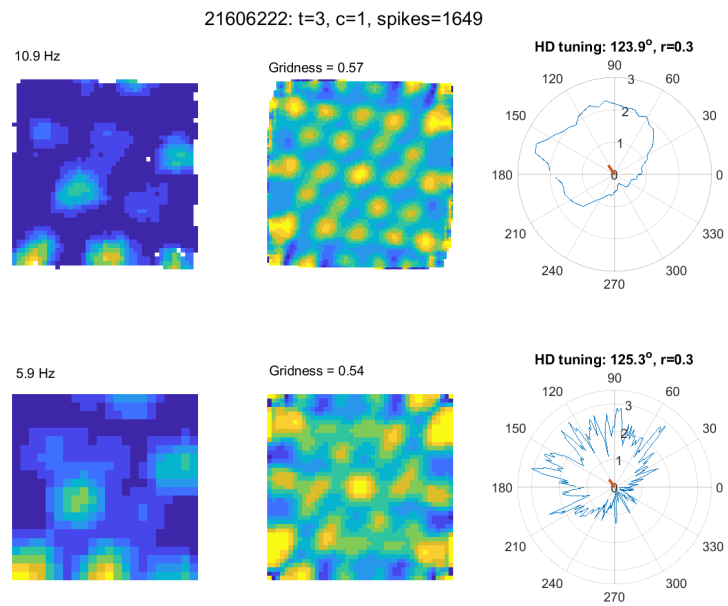


Figure 25

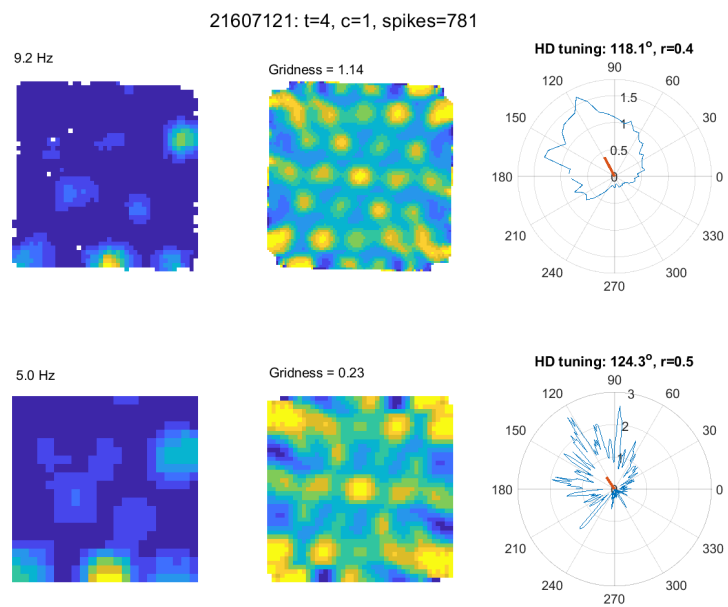


Figure 26

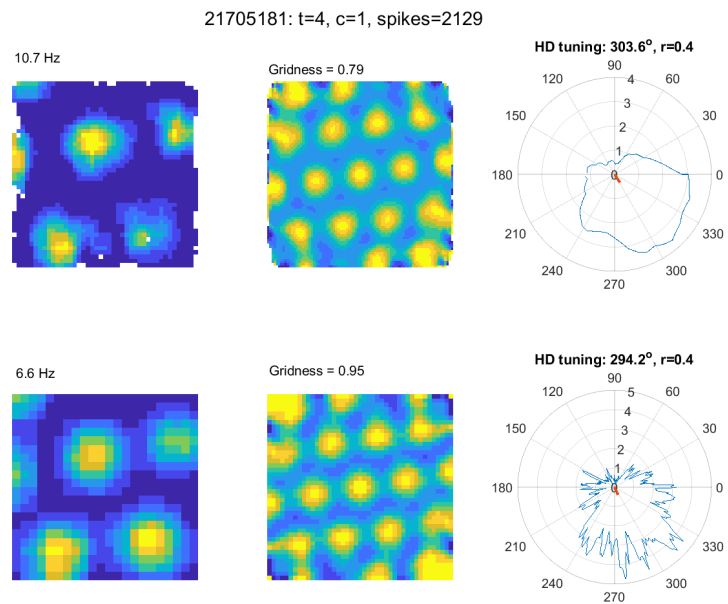


Figure 27

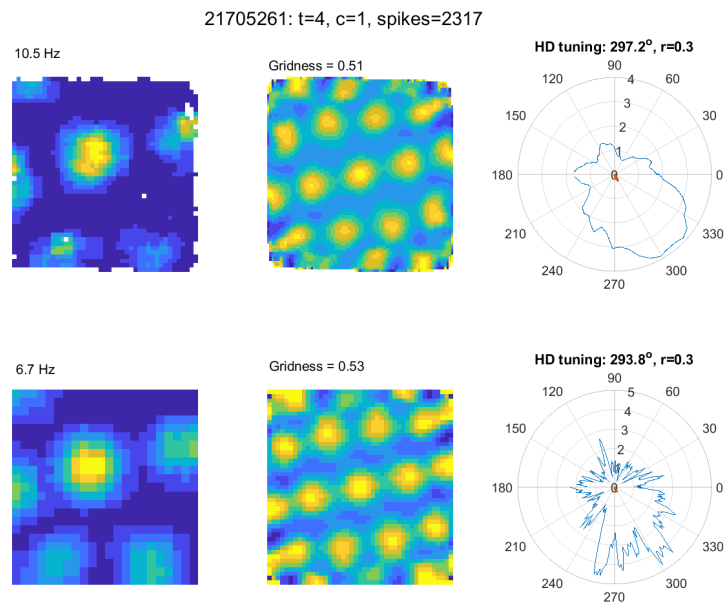


Figure 28

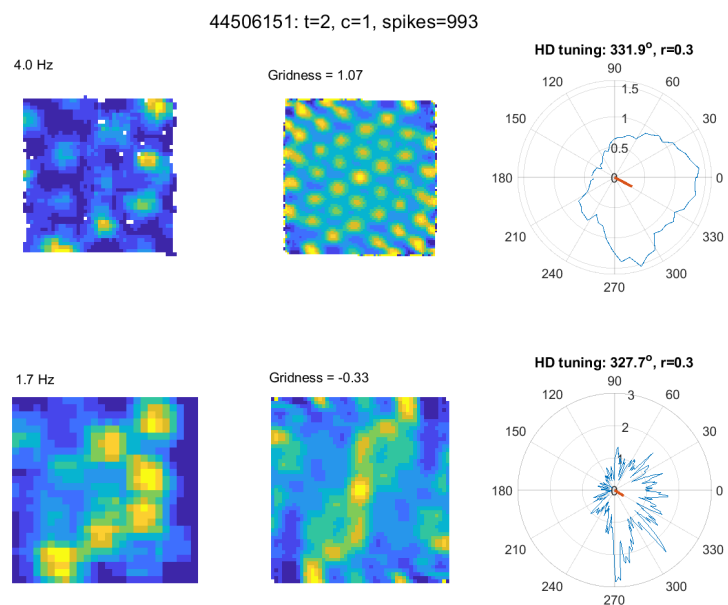


Figure 29

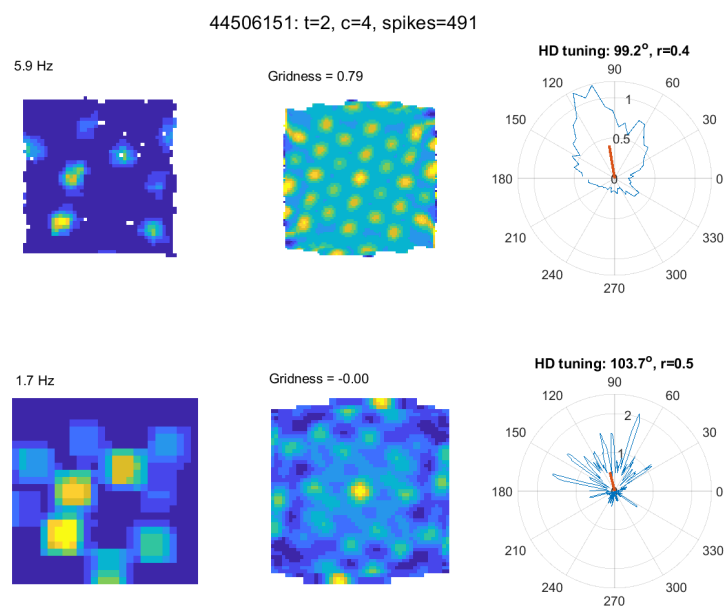


Figure 30

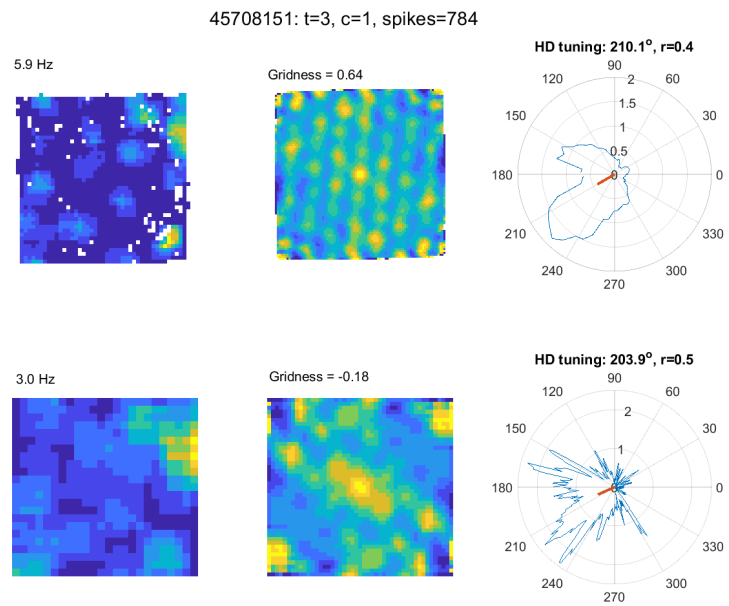


Figure 31

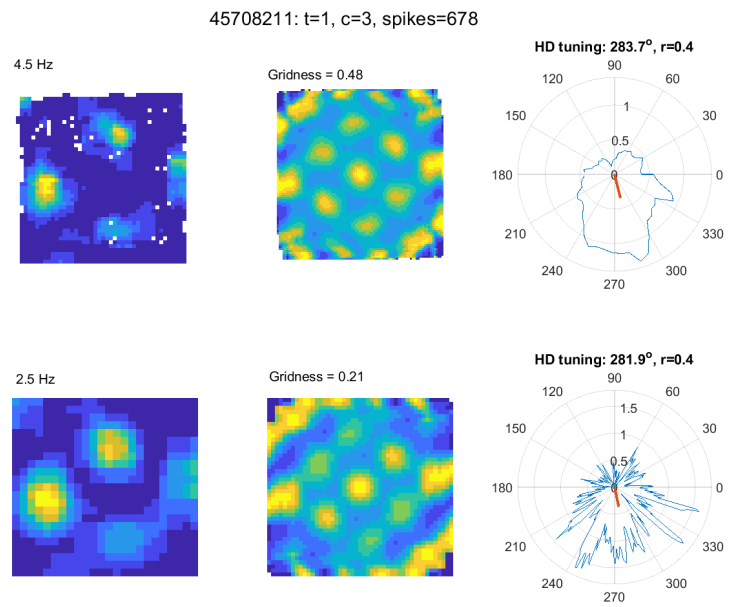


Figure 32

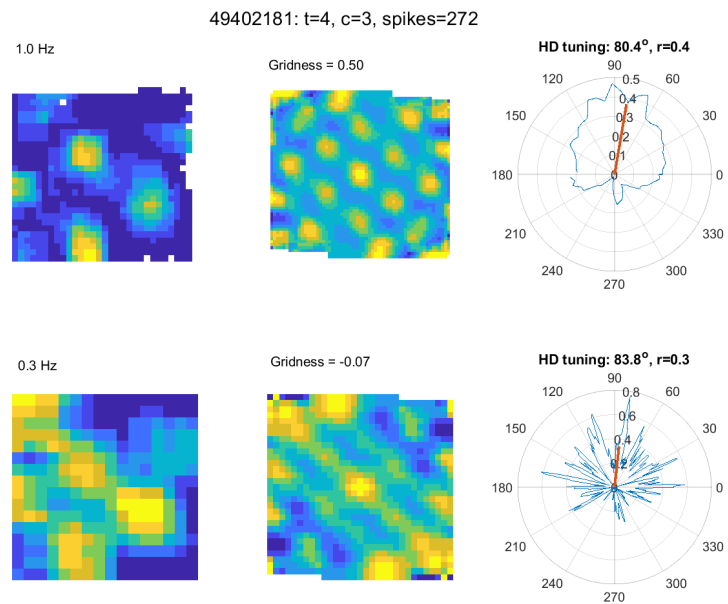


Figure 33

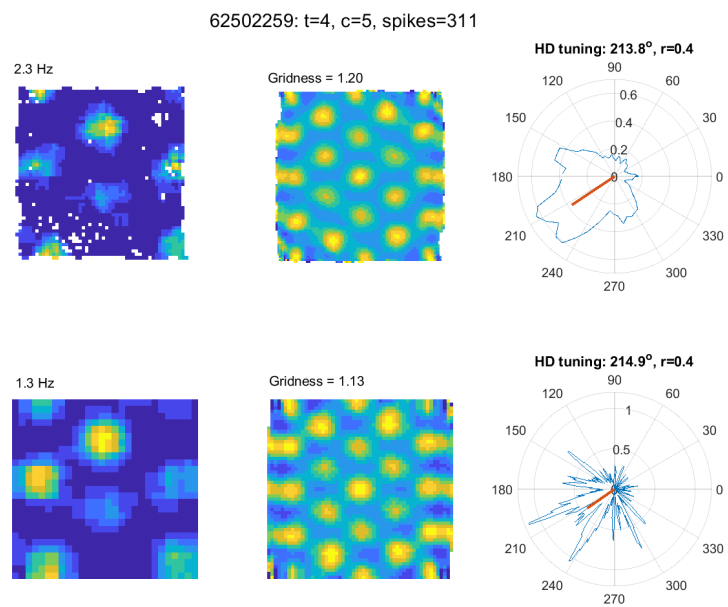


Figure 34